

This content has been downloaded from IOPscience. Please scroll down to see the full text.

Download details:

IP Address: 18.223.196.112

This content was downloaded on 11/05/2024 at 22:28

Please note that [terms and conditions apply](#).

You may also like:

[Computational Intelligence Based Solutions for Vision Systems](#)

[Accurate Exercise Recommendation Based on Multidimensional Feature Analysis](#)

Shu Zhang, Jiaqi Cai, Bin Zhuge et al.

[Comparing students' flow states during apparatus-based versus video-based lab activities](#)

Anna Karelina, Eugenia Ektina, Peter Bohacek et al.

[Measurement of cardiac output during exercise in healthy, trained humans using lithium dilution and pulse contour analysis](#)

Adrian D Elliott, Justin Skowno, Mahesh Prabhu et al.

[Metabolic Health Monitoring By Continuous Sensing of Breath Acetone at ppb](#)

Ines C. Weber, Nina Derron, Philipp A. Gerber et al.

[A Novel Portable Breath Acetone Analyzer Using a MEMS Gas Sensor Array for Fat Loss Monitoring](#)

Hyung Ju Park, Myung-Joon Kwack, Hyung-Kun Lee et al.

# Chapter 1

## How well defined are rotations in nuclei?

*Rotational states in nuclei, their symmetries and their quantum numbers are introduced. The symmetric top model and its energies and electric quadrupole,  $E2$  properties are confronted with data. The roles of spherical tensor operators, Clebsch–Gordan coefficients and the Wigner–Eckart theorem are explained. The subtle nature of the quantum mechanical uncertainty associated with rotations is illustrated. Rotational-particle coupling is defined, its main features are explored, and a data-based view is presented. A first look is taken at the peculiarities of nuclear moments of inertia.*

**Concepts:** energy patterns, total spin quantum number,  $K$  quantum number, state vectors, electric quadrupole ( $E2$ ) properties, symmetric top model, intrinsic quadrupole ( $Q_0$ ) parameter, spherical tensor operators, Clebsch–Gordan coefficients, Wigner–Eckart theorem, body frame, laboratory frame, quantum mechanical uncertainty,  $E2$  transitions, lifetimes, rotational-particle coupling, Coriolis and recoil terms, rotation alignment, moment of inertia, deformation parameter, super-deformed band, rigid and irrotational flow.

**Learning outcomes:** the key data view from this chapter is the widespread evidence for simple symmetric rotor behaviour in many nuclei. Liquid-drop behaviour of nuclei is contradicted by the emergence of constant intrinsic quadrupole moments with increasing nuclear rotational angular momentum; indeed, constancy of intrinsic quadrupole moments may be realized at the few percent level. Such constancy is not matched by rotational energy patterns, i.e. nuclei do not exhibit simple analogues of classical moments of inertia. Furthermore, coupling an odd particle spin to a rotor core angular momentum does not show the quantum mechanical analogue of classical Coriolis effects.

Rotations are widely identified in nuclei and their existence is not in question. But just what is rotating is an open question: beyond a conformity to the simplest model expressions, data indicate a variety of features for which there are only emerging

ideas and there is no consensus on interpretation<sup>1</sup>. In this chapter, we progressively look at data to see what we can and cannot say about nuclear rotation.

## 1.1 Even–even nuclei: energies and electric quadrupole, $E_2$ properties

The simplest criterion for assessing nuclear rotation is a comparison of the energies of ground-state bands of even–even nuclei with the formula,

$$E_I = AI(I + 1), \quad (1.1)$$

where  $I$  is the spin of the state,  $I = 0, 2, 4, 6, \dots$  and  $A$  is a free parameter. This leads to the familiar ratio test,  $E_4/E_2 = 3.333$  (also  $E_6/E_2 = 7.000$ , etc). Excited bands and bands in odd and odd–odd nuclei can be tested in a similar manner, allowing for a band-head excitation and non-zero spin of the band head. At a deeper level, a band can be assigned a  $K$  quantum number and electromagnetic properties can be assigned to states in a band, e.g., as an intrinsic quadrupole moment,  $Q_0$ .

The simplicity<sup>2</sup> of the energy patterns defined above for the ground-state bands of even–even nuclei demands a simple explanation. It is manifested in the symmetric top model<sup>3</sup> which is depicted in figure 1.1. This view of deformed even–even nuclei steps beyond all the details of the tens to hundreds of nucleons involved and recognizes that there is an axis of rotational symmetry and a plane of reflection symmetry at right angles to this axis. The axis of rotational symmetry has the consequence that the projection of the total nuclear spin on this axis is a constant of motion. This can be assigned a quantum number, traditionally labelled by  $K$ . The plane of reflection symmetry dictates that there is a two-fold energy degeneracy with respect to the  $K$  quantum number: the states  $|+K\rangle$  and  $|−K\rangle$  are indistinguishable energetically. Fundamentally, when such a degeneracy arises in a quantum mechanical system, a linear combination must be adopted to describe the system. Failure to do this would result in writing a state vector, e.g.  $|+K\rangle$  that would

---

<sup>1</sup> Caution is needed when attempting to conceptualize quantized rotations: quantization results in stationary states, often visualized as standing waves. In atoms, this results in the iconic atomic electron density distributions, labelled by angular momentum quantum numbers, represented using spherical harmonics. Recent studies of ultrafast pulsed laser imaging of molecules report on observations that endeavour to sharpen our view of quantized rotations [1–3]; but it is impossible to escape the limitation of only ever forming probability density ‘images’. Nevertheless, we will revisit this issue in various ways in the coming narrative.

<sup>2</sup> The simplicity of the ‘even-spins only’ property of symmetric tops with a plane of reflection symmetry is worth a deeper consideration. These are quantum mechanical systems, ranging from molecules to nuclei, possessing a fundamental symmetry. In the spectroscopy of such systems, the odd-spin states are ‘missing’. This has been the basis of searches for exotica, i.e. physical entities (particles) that have found a ‘refuge’ in symmetric top systems with the result that odd-spin states are manifested (weakly, the species are presumably rare) in the spectra. Such systems also provide a ‘laboratory’ for testing the symmetrization postulate applied to identical particles: just suppose that so-called ‘identical’ particles are not quite identical. We recommend to the reader the following: [4–8].

<sup>3</sup> The symmetric top model is a model of a rigid rotor with two components of the inertia tensor equal. This is characteristic of extended rigid bodies with an axis of rotational symmetry. A symmetric top can have a plane of reflection symmetry or reflection asymmetry through the centre of mass of the body at right angles to the axis of rotational symmetry.

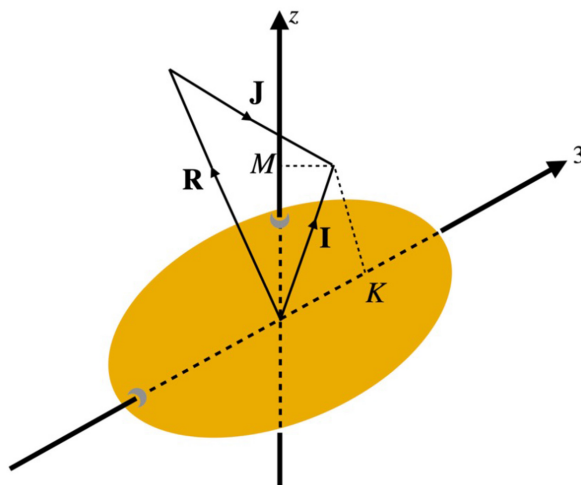


**Figure 1.1.** The quantum numbers of the symmetric top model superimposed on a schematic view of an axially symmetric deformed object, with a plane of reflection symmetry through the centre of mass at right angles to the symmetry axis. The symmetry axis is in the body-fixed frame and is labelled ‘3’. A laboratory-fixed frame axis, labelled  $z$  is also shown. Quantization of the total spin of the system,  $I$  can only be assigned sharp values for one directional component, independently with respect to the body-fixed axis and with respect to the laboratory-fixed axis, i.e. the 3-axis and the  $z$ -axis are not in any fixed relationship to each other. This relationship is not defined for a quantum mechanical rotor: a depiction of this uncertainty is attempted in figure 1.6. Thus, there are quantum numbers  $K$  (body frame) and  $M$  (lab frame), which independently range over the values  $+I, +I - 1, \dots, -I$ , respectively. The total spin  $\mathbf{I}$  of the system has an intrinsic contribution  $\mathbf{J}$  and a rotational contribution  $\mathbf{R}$ ; these are discussed further in the text. The vector  $\mathbf{R}$  is directed at right angles to the 3-axis.

imply the direction of  $K$  was known to be ‘positive’, which is an impossibility: there is no measurement which can establish this. Thus, we write

$$|IMK\rangle = \frac{\{|IM, +K\rangle + (-1)^{I+K}|IM, -K\rangle\}}{\sqrt{2}}, \quad (1.2)$$

where  $I$  is the total nuclear spin,  $K$  is the projection of  $I$  on the nuclear symmetry axis, and  $M$  is a directional component of spin in the laboratory-fixed frame of reference. The phase factor appearing in equation (1.2) applies to a plane of reflection symmetry; if the body has a plane of reflection asymmetry (through the centre of mass at right angles to the symmetry axis), there is a minus sign instead of a plus sign between the two state kets. The distinction of a body-fixed frame from the laboratory-fixed frame is discussed in detail in section 1.2. The key point here is that if  $K = 0$ , the state vector components  $|IM, +K\rangle$  and  $|IM, -K\rangle$  are indistinguishable; thus, in equation (1.2) only even values of  $I$  can occur.

Energies are observed to deviate from equation (1.1), in a smooth systematic manner. There are many formulae that attempt to describe these deviations. The simplest is

$$E_I = AI(I + 1) + BI^2(I + 1)^2, \quad (1.3)$$

where  $A$  and  $B$  are free parameters. There are other formulae expressed in terms of polynomials in  $I$ , formulae expressed using what is termed a rotational frequency, and formulae invoking parameterizations of the moment of inertia (manifested in the  $A$  parameter, above); these formulae generally have no basis in quantum mechanics, i.e., they are motivated from classical mechanics, or they are even purely mathematical with no physics motivation. To enumerate this aspect of the modelling of nuclear rotations would be laborious, inconclusive with respect to the physics involved, and indeed a distraction from the focus that we adopt herein. None of these phenomenological refinements describe the observed energies exactly. We will return to energy patterns in rotational bands shortly.

Electromagnetic properties show a remarkable conformity to the simplest quantum mechanical models in nearly all nuclei which exhibit collective behaviour. This is the starting point for the focus that we adopt. The prototype relationships are for  $B(E2)$  values of transitions and electric quadrupole moments in the ground-state bands of strongly deformed even–even nuclei, expressed as matrix elements of the electric quadrupole operator,  $T(E2)$ .

For  $B(E2)$  values, in ground-state bands of even–even nuclei, which have  $K = 0$ ,

$$B(E2; I \rightarrow I - 2) = \frac{\langle I0|T(E2)|I - 2, 0\rangle^2}{(2I + 1)}, \quad (1.4)$$

where

$$\langle I0|T(E2)|I - 2, 0\rangle = (2I + 1)^{1/2}(5/16\pi)^{1/2}\langle I020|I - 2, 0\rangle eQ_0, \quad (1.5)$$

$\langle I020|I - 2, 0\rangle$  is a Clebsch–Gordan coefficient,  $e$  is the fundamental unit of electric charge and  $Q_0$  is a model parameter describing the intrinsic quadrupole moment of the nucleus. Note, cf equation (1.2), the states are expressed in terms of the  $I$  and  $K$  quantum numbers, viz.  $|IK\rangle$ , with the  $M$  quantum number omitted because these processes are independent of the orientation of the nucleus with respect to the laboratory frame. This leads to the practical relationship, for  $B(E2; I \rightarrow I - 2) := B_{I,I-2}$ ,

$$\frac{B_{I,I-2}}{B_{20}} = \frac{15I(I - 1)}{2(2I - 1)(2I + 1)} := f(I) \quad (1.6)$$

and the leading value,  $B_{42}/B_{20} = 10/7 = 1.429$ .

For electric quadrupole moments in ground-state bands of even–even nuclei there is a dependence on the orientation of the nucleus with respect to the laboratory frame. By convention,

$$\begin{aligned} \langle IMK|T(E2)|IMK\rangle &= \langle I, M = I|T(E2)|I, M = I\rangle \langle I, K = 0|T(E2)|I, K = 0\rangle \\ &= \langle II20|II\rangle \langle I020|I0\rangle (2I + 1)^{1/2}(5/16\pi)^{1/2} eQ_0, \end{aligned} \quad (1.7)$$

whence

$$Q(I) = -\frac{I}{2I+3}eQ_0. \quad (1.8)$$

A relationship between  $B_{20}$  and  $Q(2)$  follows:

$$Q(2) = -\frac{2}{7}\sqrt{16\pi B_{20}}. \quad (1.9)$$

Equation (1.6) is applied to data in table 1.1 and figure 1.2. Equation (1.9) is applied to data in figure 1.3. The data shown are consistent with these simple relationships. Experimental uncertainties result in an unclear view of the limitations of these equations; but the averaged behaviour strongly supports nuclear rotation with a constant quadrupole moment as a function of increasing spin. While the relationships presented above are just stated here, the reader who wishes to explore how they are derived is directed to exercise 1-15.

An important implication of table 1.1 and figure 1.2 is that the model parameter  $Q_0$  is consistent with being independent of  $I$ . In contrast, changes in the rotational energy parameter,  $A$  with respect to  $I$ , viz.

$$A = \frac{\Delta E_{I,I-2}}{4I-2} = \frac{E_\gamma(I \rightarrow I-2)}{4I-2}, \quad (1.10)$$

variations of which are shown in figure 1.4, indicate that something must be changing as the nucleus ‘rotates’. But the constancy of  $Q_0$  with increasing spin implies that it is not the deformation. This implication is not widely appreciated: many authors refer to centrifugal stretching of the moment of inertia, which is naturally based on a semi-classical view of the nucleus as a liquid drop. The view of the nucleus as a rotating liquid drop is evidently wrong. Phenomenological energy formulae do not reveal the origin of departures from equation (1.1). We address the interpretation of  $A$  in terms of a moment of inertia in section 1.4. We place the word ‘rotates’ in quotation marks because we will see that even the basic concept of rotation may not be correct.

Equation (1.1) emerges from the elementary model called the symmetric top. Details are presented in section 5.3 of [9]. It is the simplest possible view of quantum mechanical rotations and only assumes an axially symmetric shape with a plane of reflection symmetry at right angles to the symmetry axis for distribution of mass within the body. No internal degrees of freedom are assigned to the body; it is a rigid body. This simplicity appears valid for the distribution of electrical charge within the body, i.e., the distribution of the protons. We will progressively address this contradiction between the model parameters  $A$  and  $Q_0$  as we proceed to look in depth at data.

Equations (1.5)–(1.9) depend on the concept of the  $K$  quantum number in association with the symmetric top. It is important to emphasize that this quantum number is a consequence of self-organization of a nuclear many-body system. These equations are the result of applying the Wigner–Eckart theorem to operators expressed in terms of the  $su(2)$  angular momentum algebra associated with nuclear

**Table 1.1.** Table of  $E2$  transition strengths in W.u. for ground-state bands of deformed even–even rare earth nuclei, showing currently known values up to  $I = 10$ . The four right-hand columns give ‘reduced’ values, where for each nucleus the  $4 \rightarrow 2$ ,  $6 \rightarrow 4$ ,  $8 \rightarrow 6$ , and  $10 \rightarrow 8$  values are scaled to the  $B(E2; 2 \rightarrow 0) = B_{20}$  value and to the rotor spin factor  $f(I)$ , given by equation (1.6). The spin factor for the  $4 \rightarrow 2$  transition is 1.429 and is noted in the column heading, with the other spin factors also given. Thus, for  $^{154}\text{Sm}$ — $245/176 \times 1.429 = 0.97$ ; with the generic form of the ratios expressed as  $B_{I,I-2}/B_{20}f(I)$ . The average value appearing in each column is given at the bottom, and the global average is 1.035, i.e., the rotor is realized at the 3.5% level. The data are taken from ENSDF (<http://www.nndc.bnl.gov/ensdf/>).

	$B(E2; I \rightarrow I - 2)$ (W.u.)					$B_{I,I-2}/B_{20}f(I)$			
	$2 \rightarrow 0$	$4 \rightarrow 2$	$6 \rightarrow 4$	$8 \rightarrow 6$	$10 \rightarrow 8$	4 1.429	6 1.573	8 1.647	10 1.692
$^{154}\text{Sm}$	176 <sup>1</sup>	245 <sup>6</sup>	289 <sup>8</sup>	319 <sup>17</sup>	314 <sup>16</sup>	0.97 <sup>2</sup>	1.04 <sup>3</sup>	1.10 <sup>6</sup>	1.05 <sup>5</sup>
$^{156}\text{Gd}$	189 <sup>3</sup>	264 <sup>4</sup>	295 <sup>8</sup>	320 <sup>17</sup>	314 <sup>14</sup>	0.98 <sup>2</sup>	0.99 <sup>4</sup>	1.03 <sup>5</sup>	1.01 <sup>4</sup>
$^{158}\text{Gd}$	198 <sup>5</sup>	290 <sup>4</sup>	—	330 <sup>30</sup>	340 <sup>30</sup>	1.02 <sup>3</sup>	—	1.01 <sup>9</sup>	1.01 <sup>9</sup>
$^{158}\text{Dy}$	186 <sup>4</sup>	266 <sup>15</sup>	340 <sup>40</sup>	340 <sup>70</sup>	320 <sup>50</sup>	1.00 <sup>6</sup>	1.16 <sup>24</sup>	1.11 <sup>23</sup>	1.02 <sup>16</sup>
$^{160}\text{Dy}$	196 <sup>3</sup>	285 <sup>11</sup>	238 <sup>13</sup>	328 <sup>30</sup>	329 <sup>15</sup>	1.02 <sup>5</sup>	0.78 <sup>5</sup>	1.03 <sup>9</sup>	1.00 <sup>5</sup>
$^{162}\text{Dy}$	204 <sup>3</sup>	289 <sup>12</sup>	301 <sup>17</sup>	346 <sup>17</sup>	350 <sup>23</sup>	0.99 <sup>4</sup>	0.94 <sup>5</sup>	1.03 <sup>5</sup>	1.01 <sup>7</sup>
$^{164}\text{Dy}$	211 <sup>4</sup>	271 <sup>11</sup>	303 <sup>9</sup>	300 <sup>13</sup>	358 <sup>18</sup>	0.90 <sup>5</sup>	0.91 <sup>3</sup>	0.86 <sup>4</sup>	1.00 <sup>5</sup>
$^{158}\text{Er}$	129 <sup>9</sup>	186 <sup>6</sup>	246 <sup>8</sup>	298 <sup>10</sup>	250 <sup>40</sup>	1.01 <sup>7</sup>	1.21 <sup>9</sup>	1.40 <sup>10</sup>	1.15 <sup>18</sup>
$^{160}\text{Er}$	169 <sup>6</sup>	241 <sup>8</sup>	263 <sup>15</sup>	290 <sup>90</sup> <sub>60</sub>	290 <sup>70</sup>	1.00 <sup>4</sup>	0.99 <sup>4</sup>	0.99 <sup>6</sup>	1.0 <sup>3</sup>
$^{164}\text{Er}$	206 <sup>5</sup>	260 <sup>30</sup>	—	343 <sup>19</sup>	353 <sup>18</sup>	0.88 <sup>10</sup>	—	1.01 <sup>6</sup>	1.01 <sup>5</sup>
$^{166}\text{Er}$	217 <sup>15</sup>	312 <sup>11</sup>	370 <sup>20</sup>	373 <sup>14</sup>	390 <sup>17</sup>	1.01 <sup>7</sup>	1.08 <sup>10</sup>	1.04 <sup>8</sup>	1.06 <sup>8</sup>
$^{168}\text{Er}$	213 <sup>4</sup>	319 <sup>9</sup>	424 <sup>18</sup>	354 <sup>13</sup>	308 <sup>13</sup>	1.05 <sup>4</sup>	1.27 <sup>5</sup>	1.01 <sup>4</sup>	0.85 <sup>4</sup>
$^{162}\text{Yb}$	135 <sup>4</sup>	210 <sup>9</sup>	191 <sup>12</sup>	250 <sup>70</sup>	180 <sup>60</sup>	1.09 <sup>4</sup>	0.90 <sup>7</sup>	1.1 <sup>3</sup>	0.8 <sup>3</sup>
$^{164}\text{Yb}$	162 <sup>5</sup>	259 <sup>9</sup>	276 <sup>10</sup>	320 <sup>110</sup>	300 <sup>120</sup>	1.12 <sup>4</sup>	1.08 <sup>5</sup>	1.2 <sup>4</sup>	1.1 <sup>4</sup>
$^{166}\text{Yb}$	191 <sup>10</sup>	272 <sup>9</sup>	291 <sup>12</sup>	320 <sup>40</sup>	310 <sup>160</sup>	1.00 <sup>6</sup>	0.97 <sup>6</sup>	1.02 <sup>14</sup>	1.0 <sup>5</sup>
$^{172}\text{Yb}$	212 <sup>2</sup>	301 <sup>20</sup>	320 <sup>30</sup>	400 <sup>40</sup>	375 <sup>23</sup>	0.99 <sup>7</sup>	0.96 <sup>10</sup>	1.15 <sup>12</sup>	1.05 <sup>6</sup>
$^{174}\text{Yb}$	201 <sup>7</sup>	280 <sup>9</sup>	370 <sup>50</sup>	388 <sup>21</sup>	335 <sup>22</sup>	0.97 <sup>4</sup>	1.17 <sup>16</sup>	1.17 <sup>7</sup>	0.99 <sup>5</sup>
$^{176}\text{Yb}$	183 <sup>7</sup>	270 <sup>25</sup>	298 <sup>22</sup>	300 <sup>50</sup>	320 <sup>30</sup>	1.03 <sup>9</sup>	1.04 <sup>8</sup>	1.00 <sup>17</sup>	1.03 <sup>10</sup>
$^{166}\text{Hf}$	128 <sup>7</sup>	202 <sup>7</sup>	221 <sup>13</sup>	280 <sup>30</sup>	—	1.10 <sup>5</sup>	1.10 <sup>9</sup>	1.33 <sup>14</sup>	—
$^{168}\text{Hf}$	154 <sup>7</sup>	244 <sup>12</sup>	285 <sup>18</sup>	350 <sup>50</sup>	370 <sup>60</sup>	1.11 <sup>7</sup>	1.18 <sup>10</sup>	1.4 <sup>2</sup>	1.4 <sup>2</sup>
$^{170}\text{Hf}$	182 <sup>7</sup>	263 <sup>4</sup>	306 <sup>10</sup>	344 <sup>12</sup>	375 <sup>25</sup>	1.01 <sup>5</sup>	1.07 <sup>5</sup>	1.15 <sup>6</sup>	1.22 <sup>8</sup>
$^{178}\text{Hf}$	160 <sup>3</sup>	—	219 <sup>12</sup>	237 <sup>6</sup>	257 <sup>8</sup>	—	0.87 <sup>6</sup>	0.90 <sup>3</sup>	0.95 <sup>4</sup>
$^{180}\text{Hf}$	155 <sup>2</sup>	230 <sup>40</sup>	219 <sup>16</sup>	245 <sup>13</sup>	238 <sup>12</sup>	1.0 <sup>2</sup>	0.90 <sup>7</sup>	0.96 <sup>5</sup>	0.91 <sup>5</sup>
$^{170}\text{W}$	124 <sup>3</sup>	179 <sup>18</sup>	189 <sup>14</sup>	190 <sup>50</sup>	170 <sup>40</sup>	1.01 <sup>10</sup>	0.97 <sup>7</sup>	0.9 <sup>2</sup>	0.8 <sup>2</sup>
$^{172}\text{W}$	171 <sup>15</sup>	245 <sup>18</sup>	260 <sup>30</sup>	290 <sup>30</sup>	270 <sup>40</sup>	1.00 <sup>9</sup>	0.97 <sup>11</sup>	1.03 <sup>14</sup>	0.93 <sup>15</sup>
$^{174}\text{W}$	135 <sup>9</sup>	235 <sup>12</sup>	410 <sup>80</sup>	240 <sup>30</sup>	160 <sup>30</sup>	1.22 <sup>9</sup>	1.9 <sup>4</sup>	1.08 <sup>13</sup>	0.70 <sup>13</sup>
$^{182}\text{W}$	136 <sup>2</sup>	196 <sup>10</sup>	201 <sup>22</sup>	209 <sup>18</sup>	203 <sup>19</sup>	1.01 <sup>5</sup>	0.94 <sup>9</sup>	0.93 <sup>8</sup>	0.88 <sup>8</sup>
$^{184}\text{W}$	120 <sup>2</sup>	166 <sup>9</sup> <sub>5</sub>	181 <sup>6</sup>	185 <sup>5</sup>	220 <sup>220</sup> <sub>130</sub>	0.97 <sup>3</sup> <sub>5</sub>	0.96 <sup>4</sup>	0.94 <sup>4</sup>	1.10 <sup>6</sup> <sub>20</sub>
$^{186}\text{W}$	111 <sup>2</sup>	144 <sup>10</sup>	187 <sup>13</sup>	178 <sup>13</sup>	151 <sup>15</sup> <sub>45</sub>	0.91 <sup>6</sup>	1.07 <sup>7</sup>	0.97 <sup>7</sup>	0.8 <sup>1</sup> <sub>2</sub>
Avg.						1.014	1.051	1.063	1.010
						global average 1.035			

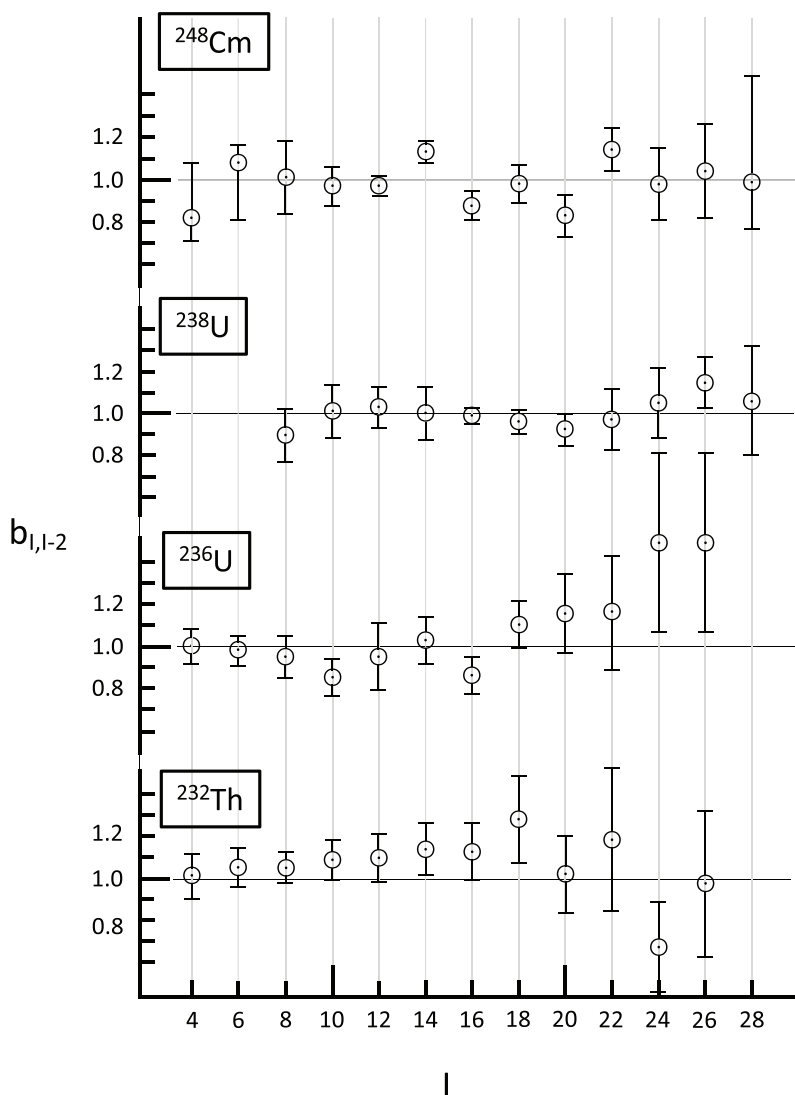


**Figure 1.2.** Values of  $b_{I,I-2} := B_{I,I-2}/B_{20}f(I)$ , where  $f(I)$  is defined in equation (1.6), for spins 4–28 for the ground-state bands of all the actinide nuclei for which there are data. If the symmetric top is valid for nuclei, all the  $b_{I,I-2}$  values should be unity.

rotation. Details of the Wigner–Eckart theorem and the  $su(2)$  algebraic structure of spin and angular momentum are presented in [10]. The band members are connected by the  $E2$  operator and the common value of  $K = 0$  for the band permits reduction of matrix elements, both transition and diagonal, to ratios of Clebsch–Gordan coefficients. The parameter,  $Q_0$  is the so-called reduced matrix element of the Wigner–Eckart theorem. There is no *a priori* reason why this should emerge from a nuclear many-body system, but it appears to work well for the most strongly



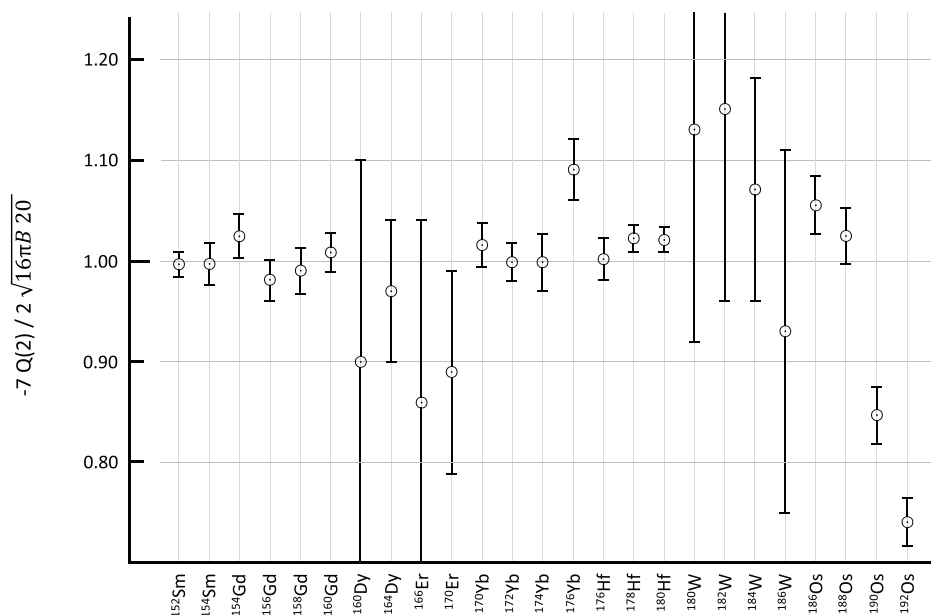


**Figure 1.3.** The ratio of  $Q(2_1^+)$  to  $\sqrt{B(E2; 2_1^+ \rightarrow 0_1^+)}$ , reduced with respect to the rotor model scale factor (see equation (1.9) and text). Rigid symmetric top behaviour would correspond to this ratio being equal to unity. See later for a discussion of <sup>186,188,190,192</sup>O<sub>s</sub>.

deformed nuclei. An introduction to the role of quantum numbers and the Wigner–Eckart theorem, in arriving at the simple relationships embodied in equations (1.5)–(1.9), is given in the next section.

## 1.2 Quantum numbers and the Wigner–Eckart theorem for nuclear rotation

The quantum numbers that label nuclear rotational states emerge from the quantum mechanics of the symmetric top model. These quantum numbers are depicted in figure 1.1. The governing quantum number of the state of a nucleus, in this context, is the total spin,  $I$ . There is a second quantum number contingent upon the value of  $I$ , its directional component. Recall that only a single directional component of  $I$  is allowed due to quantum uncertainty. Thus, one speaks of the ‘cone of indeterminacy’ in the quantum theory of angular momentum. This is depicted in figure 1.5. With respect to deformed nuclei, and specifically the symmetric top model, there are two independent frames of reference involved: the body-fixed frame and the laboratory-fixed frame. With respect to these two frames of reference, directional quantum numbers in the body-fixed frame and in the laboratory-fixed frame are defined,  $K$  and  $M$ , respectively.

The defining of two frames of reference with respect to nuclear rotation is mandatory. It is impossible to define a precise orientation of a deformed nucleus. Indeed, this is impossible for any finite many-body quantum system when any type

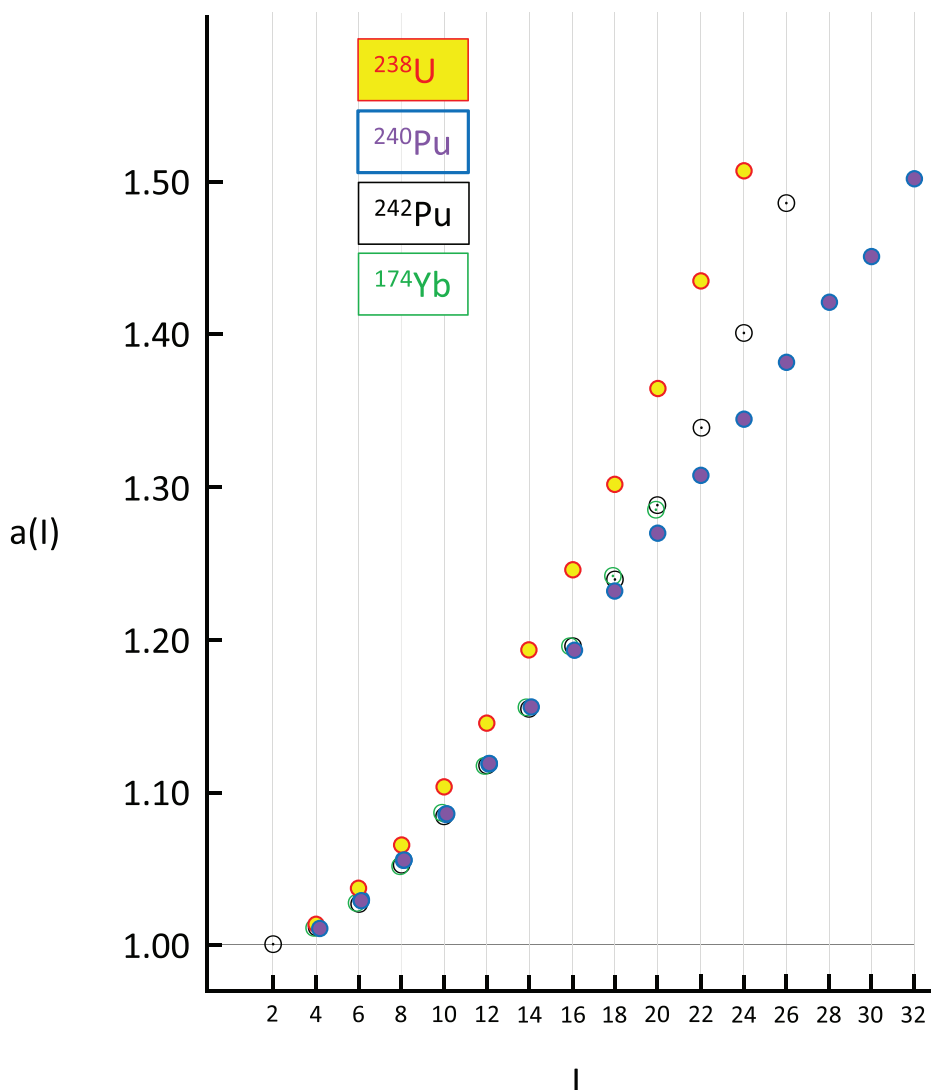


**Figure 1.4.** Values of the scaled rotational energy parameter for selected nuclei. These are defined using equation (1.10), expressed as  $a(I) := [E_\gamma(I \rightarrow I - 2)/(4I - 2)]/[E_\gamma(2 \rightarrow 0)/6]$ . A rigid rotor would result in  $a(I) = 1.000$  for all values of  $I$ . Experimental uncertainties for the input energies are too small to be shown. Note the values of  $a(I)$  for  $^{242}\text{Pu}$  and  $^{174}\text{Yb}$  are almost indistinguishable for all spin values: this is discussed further in section 1.3, including details of the uncertainty in their energies.

of ‘deformation’ of the system arises. For deformed nuclei, the two frames of reference can be viewed, in pictorial terms, as shown in figure 1.6: we refer to this view as the ‘hyper-cone of indeterminacy’. This view of the atomic nucleus underlines a fundamental limitation to our language for discussing such deformed systems: we make observations in the laboratory frame but we are describing the quantum mechanics in the body frame.

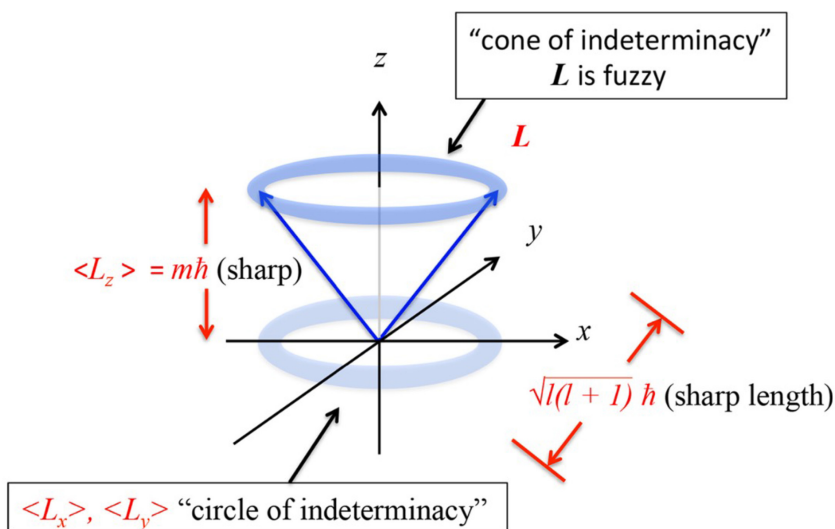


**Figure 1.5.** The ‘cone of indeterminacy’ for angular momentum in quantum mechanics. It is impossible to define more than one directional component of angular momentum, i.e. only one directional component is ‘sharp’. Thus, in physical space, the other two (Cartesian) components can only be defined to within a circle. This results in the useful depiction of the quantum mechanical uncertainty using a cone of height  $m$  and side  $\sqrt{l(l+1)}$ , in units of  $\hbar$ .

We could formulate nuclear properties entirely in laboratory-frame coordinates. The equations would be intractable. (Consider, if we attempted this when describing physical processes on the surface of the Earth as viewed from Space.) Describing physical processes occurring in systems that are rotating is enormously simplified by formulating the description in the body-fixed (rotating) frame. Note that, when this is done, so-called ‘Coriolis’ and ‘centrifugal’ effects are encountered: these are most easily viewed from the laboratory frame. (Consider, understanding a rotating air mass in a storm system and the flow of air towards the North Pole and the consequent acquisition of easterly motion, as viewed from Space looking down from above the North Pole.) We will address Coriolis and centrifugal effects in nuclei in due course (with some major surprises). (If we expressed properties of nuclei in a laboratory-frame of reference, from all the intractable equations we would find the emergence of some very simple relationships: these relationships would be difficult, even impossible to understand; but would be transparent, even trivial when expressed in a body frame of reference.)

The observational basis of nuclear spectroscopy is the determination of expectation values of quantities such as energies, spins, quadrupole moments, and transition probabilities (radiation intensities). These are formally expressed as ‘diagonal’ matrix elements of operators for expectation values and ‘transition’ matrix elements of operators for transition probabilities. In a quantum-mechanical model description, one works in a basis of energy eigenstates which possess simultaneous quantum numbers, in the present context angular momentum quantum numbers. Thus, the quantum states of the symmetric top model, in the

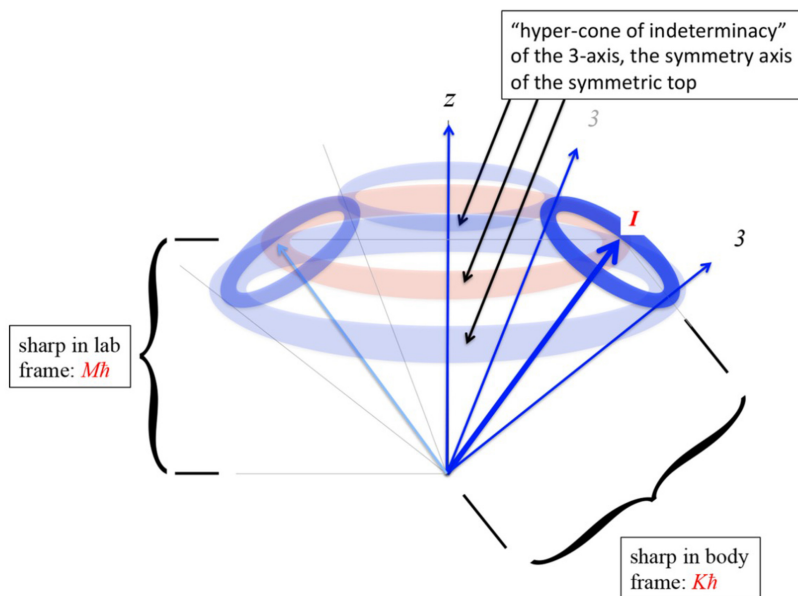


**Figure 1.6.** The ‘hyper-cone of indeterminacy’ for the quantum mechanical axially symmetric rotor. The body-fixed frame and the laboratory frame are not in a fixed relationship to each other: they are connected by the total spin  $I$  possessing a fixed projection  $M\hbar$  on the laboratory frame  $z$ -axis and a fixed projection  $K\hbar$  on the body frame 3-axis. In consequence, the 3-axis has an uncertainty that involves two cones of uncertainty from which the figure endeavours to depict the full degree of uncertainty possessed by the quantum axially symmetric rotor.

body-fixed frame, are defined by energy,  $I$ , and  $K$ , viz.  $|E, I, K\rangle$ . For present purposes, just three quantum numbers<sup>4</sup> define the entirety of the quantum mechanics of the model. Most importantly, they define the quantum mechanical basis within which all properties of the system are formulated.

Physical processes in quantum mechanical systems are described by operators. To understand how operators work (operate) within the system, one must know how the operators act on the basis states. This is variously formulated in quantum theory using differential operators acting on functions, matrices acting on vectors, or algebraic formulations. For present purposes, an algebraic formulation is by far superior in conciseness and ease of use; but it is the most abstract. We remind the reader that any formulation of quantum mechanics involves the preciseness of mathematics, with the mandate that the description cannot imply more information than is physically achievable by measurement. Herein lie the features of quantum theory that defy everyday logic.

Operators act on basis states to produce other basis states, or the same basis state: if the state is another basis state, a transition has occurred; if the state is the same basis

<sup>4</sup>There is a parity quantum number that is contingent on  $I$ , also on internal symmetries of the body: we do not discuss this here as it does not play any role; but some details are presented in [9], and later in this volume.

state, that defines an observable of the system. Transitions are also observable, but there is a profoundly subtle aspect to transitions in quantum systems: namely, we learn about quantum systems by a focus on energy eigenstates, so-called stationary states. Energy eigenstates ‘do not do anything’ within the system. For a transition to occur, the system must be coupled (interact) with another system. For nuclei this could be by collision with another nucleus. It can also be by coupling to what we call the electromagnetic vacuum. This is always present; but when a nucleus is in an excited state (an energy eigenstate), e.g. after having been produced by a nuclear collision, the excited nuclear state is not just under the control of the Hamiltonian for the nucleus; it is also coupled to the Hamiltonian for the electromagnetic vacuum. Thus, the nucleus in its excited state, while in an energy eigenstate of the nuclear Hamiltonian, is not in an energy eigenstate of the total Hamiltonian: it emits electromagnetic radiation and undergoes a transition to a new energy eigenstate of the nuclear Hamiltonian.

One might ask: ‘how come the nucleus ends up in an eigenstate of the nuclear Hamiltonian and not that of the total (nuclear + electromagnetic, field) Hamiltonian?’ The answer is that the coupling between the two is weak. If the coupling was strong, the states of the nucleus would not be observed as sharply defined energies: such states are observed in nuclei as resonances. These resonances have broad energy distributions because they are unbound with respect to neutron or proton emission; thus, one must consider such unbound states in the full basis of description and these unbound states have continuous energy distributions. In fact, due to coupling to the em vacuum, bound excited states have energy ‘widths’: these are expressed as  $\Delta E = \hbar/\tau$ , where  $\tau$  is the mean lifetime of the quantum state. For electromagnetic decay, these widths are generally far smaller than the precision with which we can measure the energies of excited states in nuclei (detector energy resolution). But such widths are seen in laser spectroscopy of excited states in atoms. Energy widths observed in meson and baryon spectroscopy are nearly all enormous, for quite different reasons than in nuclei<sup>5</sup>.

The handling of operators and how they act on basis states is enormously simplified when symmetry is possessed by the physical system. The initial and final states in any process must possess this symmetry for fast decay modes (the dominant modes). As such, we classify operators by such symmetry. An operator may or may

---

<sup>5</sup> Baryons and mesons (hadrons) exhibit excited states due to their internal quark and anti-quark degrees of freedom (and probably their gluon degrees of freedom). But quarks (and gluons) are absolutely bound. The widths come from the strong coupling of these excitation degrees of freedom to decay processes such as the emission (creation) of, e.g.  $\pi^0$  or  $\pi^+\pi^-$  pairs (a certain analogy to the internal-conversion and internal-pair decay modes in nuclei exists here). But there are a few excited states in baryon and meson systems that only have small energy widths: these are states that can only decay by the weak interaction. The historical sensation was the so-called  $J/\psi$  particle, a meson formed of a charm-anti-charm quark pair. This ‘charmonium’ system has excited states that predominantly decay by gamma-ray emission, i.e., through their coupling to the em vacuum: they also have relatively narrow widths. One can take this line of thinking back into atomic systems with the example of the ‘atom’ formed by an electron–positron pair, positronium. Positronium has singlet and triplet lowest-energy states. Unlike hydrogen, positronium has a decay channel: annihilation. The singlet and triplet lowest-energy states have different widths due to symmetry with respect to decay into two or three photons, following the annihilation process. This is a rich arena for understanding time-dependent processes related to finite bound quantum systems.

not possess this symmetry. If it does possess the symmetry, our job is almost done (see below); if it does not, we expand the operator in basis components defined by the symmetry. To put this into practical terms, electromagnetic decays of the nucleus can be expressed in terms of the spherical harmonics. We refer to this expansion as multipoles of the radiative process (coupling to the em field). While such an expansion may contain many terms (multipoles), only one or a few components in the expansion dominate. The reason is that spherical harmonics are defined also by an angular momentum-type label, and photon emission from nuclei is highly restricted by angular momentum such that a spin change of more than one or two units is very improbable (recall that the spin of a photon is  $1\hbar$ ). This is the basis of the so-called ‘Weisskopf’ estimate for electromagnetic transition strengths in nuclei.

Spherical harmonics are labelled by indices that match the mathematical structure of the angular momentum theory of quantum systems. We could say that they are ‘symmetry-adapted’. Thus, spherical harmonics appear as representations in a wave function description of electronic states in atoms. They are not simply adapted to a wave function description of nuclear rotations (because of the hyper-cone of indeterminacy, they are too sharp, i.e., they would imply more information than we possess<sup>6</sup>). But all we really need from the concept of the spherical harmonics is that of multipolarity, their indices. This takes us into the concept of the spherical tensor structure of operators, and hence to the Wigner–Eckart theorem.

Spherical tensors are mathematical entities just like scalars and vectors. One can manipulate them: add them together; operate on them, e.g. rotate a vector. But there is an over-riding constraint: a vector cannot be added to a scalar. The underlying mathematical generalization is the concept of tensorial character. A scalar has just one ‘component’, which formalizes the concept of ‘number’. A vector in the space in which we live has three components, say  $(x, y, z)$ . A four-dimensional space has vectors with four components and so on. Spherical tensors are indexed by two numbers, conventionally by  $\{l, m\}$  or  $\{\lambda, \mu\}$ : for a given  $\lambda$ ,  $\mu = +\lambda, +\lambda - 1, \dots, -\lambda$ , i.e.  $2\lambda + 1$  components. Thus, for  $\lambda = 1$ , there are three components, and such a spherical tensor is said to be isomorphic (identical in form) to a cartesian vector in three-dimensional space: this can be expressed, for  $T_{\mu}^{(\lambda)}$ , with  $\lambda = 1$ , as  $T_{+1}^{(1)} = x + iy$ ,  $T_{-1}^{(1)} = x - iy$ ,  $T_0^{(1)} = z$ . Operators can be expressed as spherical tensors, angular momentum states have identical spherical tensor structure, so there are rules for combining them.

---

<sup>6</sup> Rotational wave functions or Wigner-D functions are quite complicated. They can be expressed in their full detail as ‘arrays’ of products of pairs of spherical harmonics, sometimes appearing in a matrix form. The reason is that two directional indices must be used for quantum mechanical rotations, the earlier defined  $K$  and  $M$  quantum numbers. This double indexing, and doubly expressed uncertainty, is because the orientation of the laboratory-fixed frame of reference and the body-fixed frame of reference has an inherent quantum mechanical uncertainty, as shown in figure 1.6. Thus, we cannot use single spherical harmonics: the Wigner-D functions—arrays of products of pairs of spherical harmonics, one labelled by  $K$  and one labelled by  $M$ —express this uncertainty in precise mathematical terms. They are usually written  $D_{MK}^I(\theta, \phi)$ , where the argument of the function involves the spherical polar angles describing the orientation of the body-fixed frame with reference to the laboratory-fixed frame, indexed by the total spin  $I$ . We do not use the Wigner-D functions herein.

The quantum theory of angular momentum, whether applied to nuclei or atoms, or any other finite many-body quantum system provides rules for coupling states of angular momentum together, e.g. coupling a spin to an orbital angular momentum or coupling two particle spins together to obtain a resultant total spin. So, one can ‘couple’ a spherical tensor operator to an angular momentum state: this is how an operator can be viewed as acting on a state. One obtains a final state in a physical process, which can be viewed as coupling the ‘spin’ of the operator to the spin of the state. The rules for such coupling are governed by Clebsch–Gordan, CG, coefficients.

For the action of operators on states to produce new states (transitions within the system) this enables such processes to be formulated in terms of CG coefficients. This is expressed as

$$\langle I_f K_f | \mathbf{T}_\mu^{(\lambda)} | I_i K_i \rangle = \langle I_f K_f \lambda \mu | I_i K_i \rangle \langle I_f || \mathbf{T}^{(\lambda)} || I_i \rangle / (2I_i + 1), \quad (1.11)$$

where the term on the left is the matrix element describing the physical process, the first term on the right is a CG coefficient, and the ‘double-barred’ expression on the right is called the ‘reduced’ matrix element (the denominator on the right is a conventional factor). This is the statement of the Wigner–Eckart theorem. It provides an enormous reduction in computational labour; often just involving a look-up of the CG coefficient. Even, if the CG coefficient is zero, this leads to the concept of a ‘forbidden’ transition.

What is remarkable about the rotational states of nuclei is that in equation (1.11), the reduced matrix element is a common numerical factor for many matrix elements. Specifically, for the  $K = 0$  rotational band built on the ground state of a doubly even nucleus, all transition and all diagonal matrix elements reduce within experimental error to a single number (multiplied by a CG coefficient), which we define to be  $Q_0$ : the so-called intrinsic quadrupole moment of the nucleus. This is arguably the best manifestation of the Wigner–Eckart theorem in the entire domain of quantum theory. This ‘reduction’ depends on the validity of the quantum number  $K$ , which is a model quantum number. Note that in equation (1.11), on the right-hand side, the reduced matrix element is independent of  $K$ : one could say that the Wigner–Eckart theorem has ‘factored-out’  $K$  and isolated it in the CG coefficient.

Note that nowhere does one need to formulate the quantum mechanics of the electromagnetic field in the above details. One only needs to know that precise amounts of energy can be exchanged between the nucleus and the em field (with allowance for recoil energy of the nucleus when high-precision measurements are used); and that rates of decay, probabilities of exchange of energy, have a dependence on the angular momentum change and the parity change. For the quadrupole degree of freedom, the spin change is two, with no parity change. Again, we note the role of the Weisskopf estimates; herein combined with the observation that collective degrees of freedom exhibit large enhancements over these estimates (large  $B(E2)$  values).

The full details of the quantum mechanics underlying this section are given in the earlier volumes in this series: (chapter 9 of [11]) an introduction to time-dependent

quantum mechanics, (chapter 11 of [11]) an introduction to the algebraic structure of angular momentum and spin, (chapter 1 of [10]) spherical harmonics, (chapter 2 of [10]) coupling of angular momenta and spins, (chapter 3 of [10]) tensor structure of operators and the Wigner–Eckart theorem, (chapter 8 of [10]) time-dependent perturbation theory, (chapter 9 of [10]) the electromagnetic field in quantum mechanics. Note that handling the multipole expansion of the electromagnetic field is not yet developed in the Series (only the electric dipole approximation was made in chapter 9 of [10]); higher multipole terms will be needed, e.g. for the theory of angular correlations between sequential radiative decay steps.

### 1.3 Odd nuclei: energies and $E2$ properties

We can immediately look more deeply at the issue of rotations in nuclei by inspecting data for odd-mass nuclei. The above equations are for ground-state bands of even–even nuclei, i.e., for  $K = 0$ . For general  $K$  values these equations are modified by replacement of the CG coefficients, viz.  $\langle I020|I - 2, 0 \rangle \rightarrow \langle IK20|I - 2, K \rangle$  in equation (1.5) and  $\langle I020|I0 \rangle \rightarrow \langle IK20|IK \rangle$  in equation (1.7). For example, this leads to the relationship (cf equation (1.7))

$$Q(I, K) = \frac{[3K^2 - I(I + 1)]eQ_0}{(I + 1)(2I + 3)}. \quad (1.12)$$

Figures 1.7(a)–(f) show values of the parameter  $Q_0$  extracted from data for selected odd-mass nuclei using equation (1.4) and (cf equation (1.5))

$$\langle I, K|T(E2)|I - 2, K \rangle = (2I + 1)^{1/2}(5/16\pi)^{1/2}\langle IK20|I - 2, K \rangle eQ_0. \quad (1.13)$$

The model interpretation is again consistent with  $Q_0$  being independent of  $I$ . Comparison of  $Q_0$  values for odd-N nuclei with their even–even neighbours is shown in figure 1.8; a similar comparison for odd-Lu isotopes with even-Yb and even-Hf neighbouring isotopes is shown in figure 1.9. Figure 1.10 shows  $Q_0$  values in the actinide region. The pattern is consistent with a smooth variation in  $Q_0$  as a function of mass number. While all the even–even nuclei involve  $K = 0$  states, the odd nuclei have a range of  $K$  values; but  $Q_0$  systematics are smooth and illustrate the independence of this quantity with respect to  $K$ . This is a practical illustration of the way that the Wigner–Eckart theorem works, beyond the data showing that  $Q_0$  values are consistent with a single value in a rotational band.

Although energies of states in rotational nuclei do not conform exactly to equation (1.1), one can inspect energy patterns in neighboring nuclei to seek similarities and differences. The comparison of odd and even–even neighbours is made for  $\gamma$ -ray transition energies for selected nuclei in figures 1.11–1.13. In some cases, the differences implied for the rotational energy parameter(s) are  $\sim 0.1\%$ . In general, differences in energies between odd-mass nuclei and even–even nuclei depend on a so-called ‘rotation-particle coupling’ term. From the rotational energy Hamiltonian,

$$H = AR^2, \quad (1.14)$$



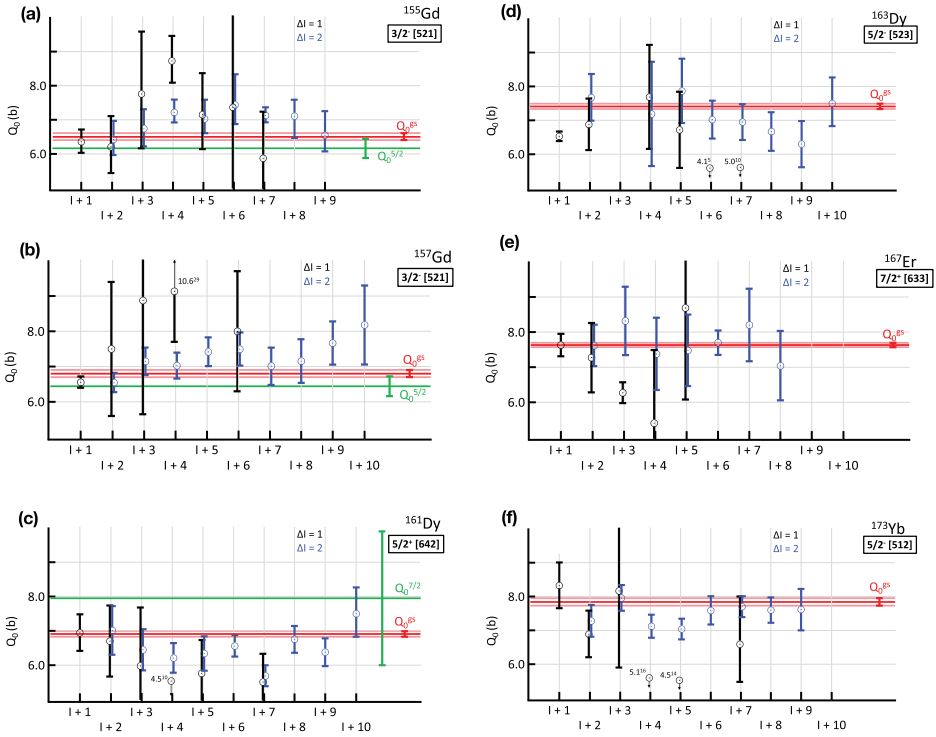


**Figure 1.7.** (a–f) Intrinsic quadrupole moments  $Q_0$  in barns versus spin for ground-state bands of selected odd- $N$  nuclei in the rare earth region, extracted using the axially symmetric rotor model, cf equations (1.4), (1.12), (1.13). These values are based on  $B(E2)$  values given in ENSDF (except for  $^{157}\text{Gd}$  where failure to use an erratum [12] results in all the ENSDF values for states with spin above  $7/2$  being wrong). The values of  $Q_0$  and their uncertainties deduced from the ground-state spectroscopic quadrupole moments are shown in red, with extension across the entire range of spins of excited states so that they form a visual base reference for each nucleus. Where excited state quadrupole moments have been measured, in  $^{155}, ^{157}\text{Gd}$ ,  $^{161}\text{Dy}$ , these are shown in green and the centroid of the value again extends across the entire range of spins of excited states, but the uncertainties are localized using standard error bar notation. The spectroscopic quadrupole moment values are taken from ENSDF and [13]. The most precise values of  $Q_0$  are for the ground states, which result from the spectroscopic quadrupole moments. Excited band members appear to be consistent with no changes in  $Q_0$  as spin increases, but the precision is insufficient to make strong statements regarding constant  $Q_0$  values for any of these bands.

where  $\mathbf{R}$  is the collective angular momentum of the core and  $A$  is the rotational energy parameter, cf equation (1.1) and figure 1.1. Then, defining

$$\mathbf{I} := \mathbf{R} + \mathbf{j}, \quad (1.15)$$

where  $\mathbf{I}$  is the total spin of the nucleus and  $\mathbf{j}$  is the spin of the odd nucleon,

$$H = A(\mathbf{I} - \mathbf{j}) \cdot (\mathbf{I} - \mathbf{j}) = AI^2 - 2A\mathbf{I} \cdot \mathbf{j} + A\mathbf{j} \cdot \mathbf{j}. \quad (1.16)$$

On quantization, this leads to

$$E = AI(I + 1) - 2A(\mathbf{I} \cdot \mathbf{j}) + A(\mathbf{j} \cdot \mathbf{j}), \quad (1.17)$$

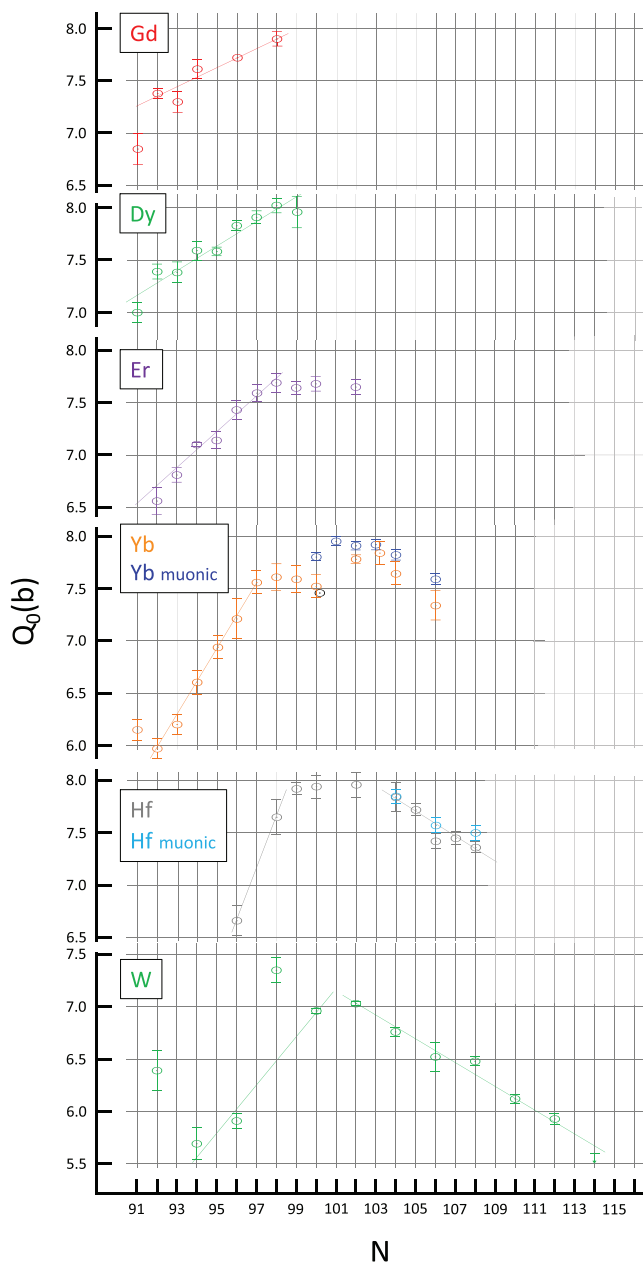


**Figure 1.8.** Comparison of  $Q_0$  values in barns for ground states in odd- $N$  nuclei and  $2_1^+$  states in even-even neighboring nuclei, Gd–Hf. Sloping lines are to suggest a more rapid onset of deformation in going from Gd to Yb. The values are computed using data taken from [ENSDF](#) and [13]. The value of  $Q_0$  for  $^{161}\text{Dy}$  is taken from the fit to the muonic hyperfine structure allowing for K mixing [14]. The two sets of values shown for some of the Yb and Hf isotopes correspond to evaluated data in [ENSDF](#) and data from muonic x-ray hyperfine structure: specifically, data from [15] and data from [16]. For  $^{170}\text{Yb}$ , three values are shown:  $Q_0^{\text{Coul.}} = 7.4617$  b [black],  $Q_0^{\text{muonic}} = 7.804$  b [blue], and  $Q_0^{\text{ENSDF}} = 7.5211$  b [orange].

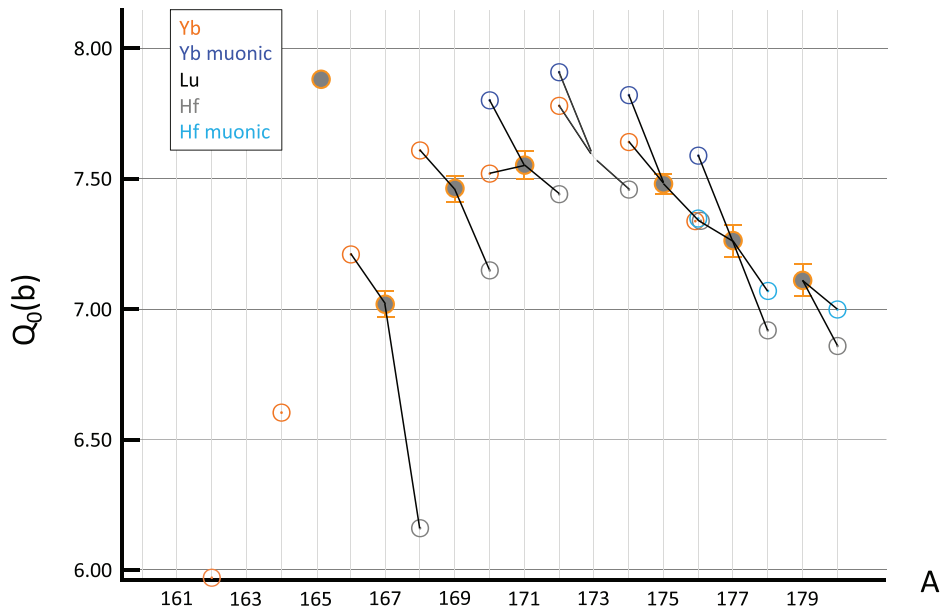


**Figure 1.9.** Comparison of  $Q_0$  values in barns for ground states in odd-Lu ( $Z = 71$ ) nuclei and  $2_1^+$  states in even-even neighboring Yb ( $Z = 70$ ) and Hf ( $Z = 72$ ) nuclei. Uncertainties are shown only for the Lu isotopes. Lines connect the Yb-Lu-Hf isotones. The values are computed using data taken from [ENSDF](#) and [\[13\]](#).

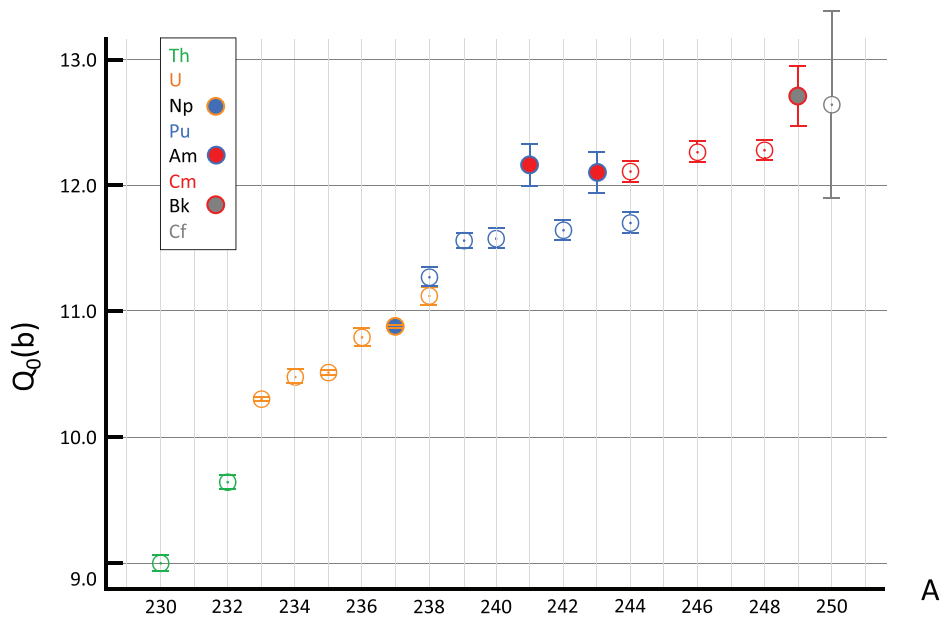


**Figure 1.10.** Comparison of  $Q_0$  values in barns for ground states in actinide nuclei. The values are computed using data taken from [ENSDF](#) and [\[13\]](#).

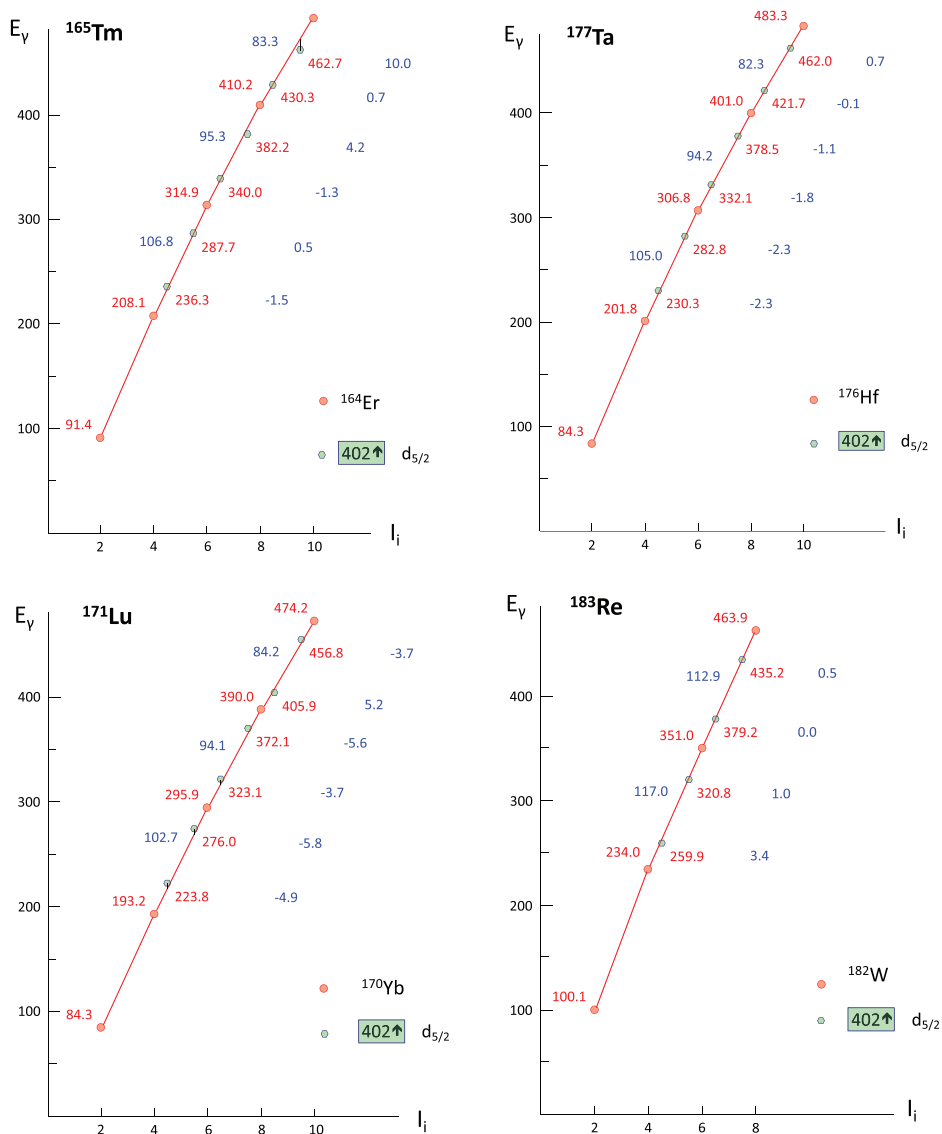


**Figure 1.11.** (a–d) Plot of  $\gamma$ -ray transition energy,  $E_\gamma$  in keV versus spin of the initial state,  $I_i$  for rotational bands built on the Nilsson state  $5/2^+ [402]$  for selected odd- $Z$  nuclei spanning  $N = 96$  to  $108$ , compared to neighbouring  $A - 1$  even-even ‘core’ nuclei. All the transitions have  $\Delta I = 2$  and the plots are limited to the lowest spin band members. Experimental values are given in red; energy differences (even mass, self-evident) or interpolated energy differences (e.g.  $106.8 \times 0.25 + 208.1 - 236.3 = -1.5$ ) are given in blue. Thus, for the odd-mass nuclei, if the difference is negative the data point lies above the even-even ‘trajectory’: this convention is in recognition of the negative sign in the RPC term in equation (1.17). Details are discussed in the text. The data are taken from [ENSDF](#).

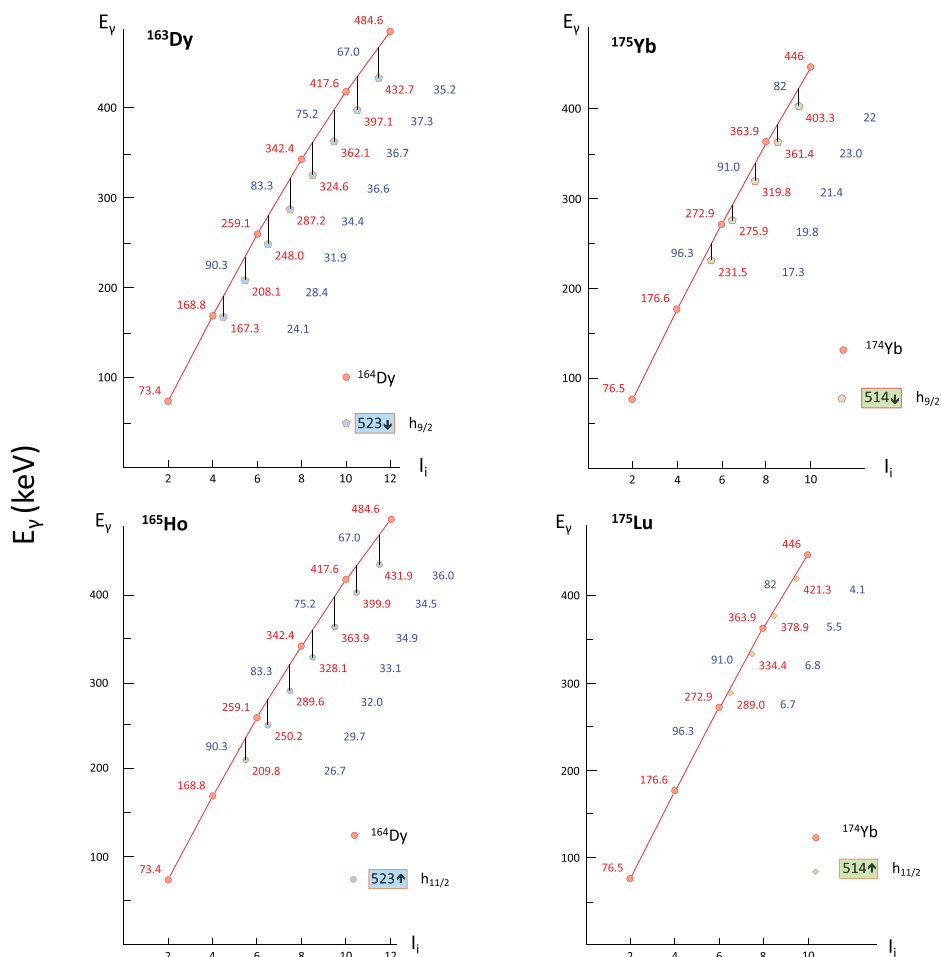


**Figure 1.12.** (a–d) Plot of  $\gamma$ -ray transition energy,  $E_\gamma$  in keV versus spin of the initial state,  $I_i$  for rotational bands built on the Nilsson states  $5/2^-$  [523] ( $^{163}\text{Dy}$ ),  $7/2^-$  [523] ( $^{165}\text{Ho}$ ) and  $7/2^-$  [514] ( $^{175}\text{Yb}$ ),  $9/2^-$  [514] ( $^{175}\text{Lu}$ ). Note the common reference cores; also note that these are unique-parity configurations involving  $l = 5$ ,  $j = 9/2 = 5 - 1/2$  (odd-neutron nuclei with  $523\downarrow$  and  $514\downarrow$ ) and  $l = 5$ ,  $j = 11/2 = 5 + 1/2$  (odd-proton nuclei with  $523\uparrow$  and  $514\uparrow$ ). For other details, see the caption to figure 1.11 and discussion in the text. The data are taken from [ENSDF](#).

where the first term is familiar, cf equation (1.1); the second term is called the ‘rotational-particle coupling’, RPC, term (also, sometimes, it is called the ‘Coriolis’ term) and the third term is called the ‘recoil’ term. These are expressed as expectation values with respect to specific states in a rotational band and are handled shortly. (The appearance of expectation values is because  $j$  is not a good quantum number in a deformed mean field, i.e.  $j$  values are mixed; this is handled later.) It is important to note that the second term is linear in  $I$  and the third term is independent of  $I$ . Thus, energy differences, notably  $E_\gamma(I \rightarrow I - 2)$  can be approximated by

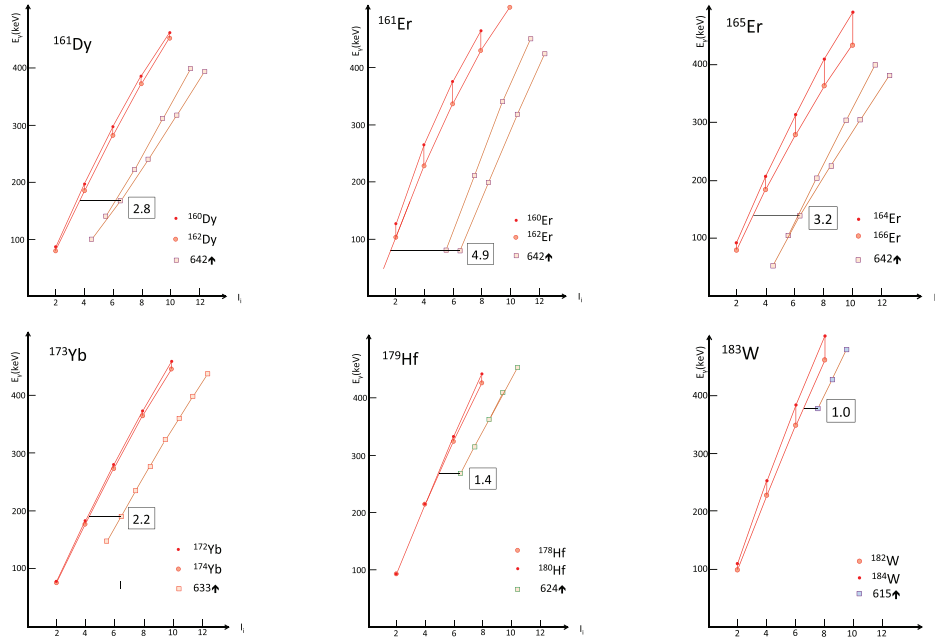


**Figure 1.13.** (a–f) Plot of  $\gamma$ -ray transition energy,  $E_\gamma$  in keV versus spin of the initial state,  $I_i$  for rotational bands built on Nilsson states originating from the  $i_{13/2}$  configuration. The ‘alignment spins’ for the  $13/2 \rightarrow 9/2$  transitions (and  $15/2 \rightarrow 11/2$  in  $^{183}\text{W}$ ) are given in the boxes. Both the  $A - 1$  and the  $A + 1$  core nuclei are shown; the alignment spins are relative to the trajectory of the core with the lower set of energies. The pattern suggests that alignment decreases with increasing  $\Omega$ , i.e.  $633\uparrow$  ( $\Omega = 7/2$ ),  $624\uparrow$  ( $\Omega = 9/2$ ),  $615\uparrow$  ( $\Omega = 11/2$ ), cf  $^{173}\text{Yb}$ ,  $^{179}\text{Hf}$ ,  $^{183}\text{W}$ , and with increasing deformation, cf  $^{161}\text{Er}/^{161}\text{Dy}$  and  $^{161}\text{Er}/^{165}\text{Er}$  (note configurations are all  $642\uparrow$  ( $\Omega = 5/2$ ) and line slopes are  $^{161}\text{Er} > ^{161}\text{Dy}$ ,  $^{161}\text{Er} > ^{165}\text{Er}$ , where line slope is fixed by rotational energy constant which is inversely proportional to the moment of inertia). Other details are explained in the caption to figure 1.11 and in the text. The data are taken from ENSDF.

$$E_\gamma(I \rightarrow I - 2) = A(4I - 2) - 2A(2j \cos \theta_{Ij}), \quad (1.18)$$

where  $\theta_{Ij}$  can be viewed as the semi-classical angle between the average  $j$  of the unpaired nucleon and the total nuclear spin,  $I$ . It is evident from figures 1.11–1.13 that the second term in equation (1.18) is indeed generally independent of  $I$ . In many nuclei it is almost zero. The largest non-zero occurrences of the second term in equation (1.18), which are for configurations originating in high  $j$ -value spherical shell model structures, and are termed ‘alignment’ energies, are shown in figures 1.14(a)–(c).

The rotation-particle coupling term in the Hamiltonian generally has a small influence on electromagnetic properties in odd-mass nuclei. However, for  $K = 1/2$  bands it can be significant. The contribution of this term to energies is discussed in chapter 3 of [9] (especially figures 3.11 and 3.12; and cf equation (3.16) therein). For  $K = 1/2$  bands and  $E2$  matrix elements

# Nuclear Data

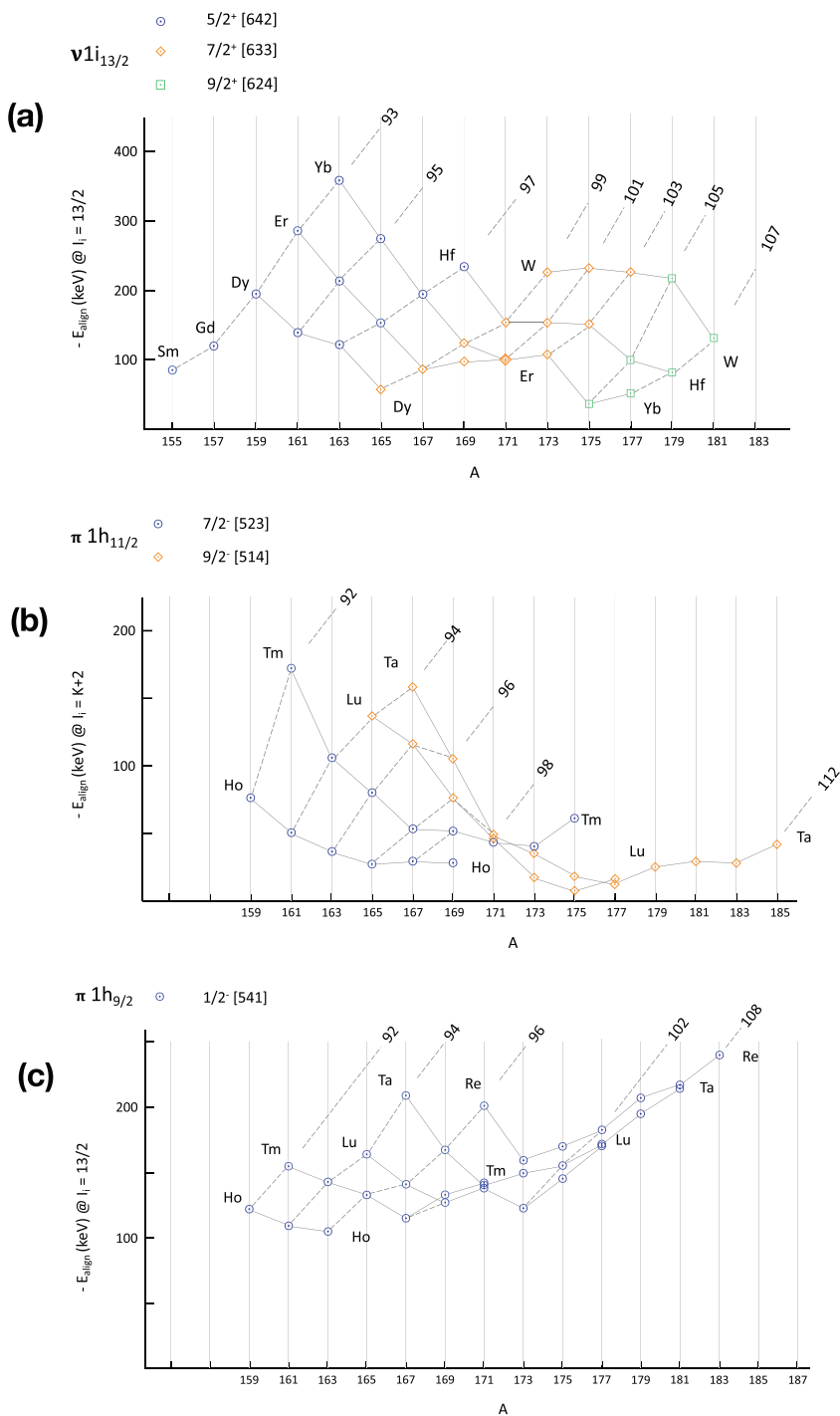


**Figure 1.14.** (a-c) Plot of ‘alignment’ energies in keV at specified spins (indicated) for bands built on Nilsson configurations from: (a) the  $1i_{13/2}$  configuration; (b) the  $1h_{11/2}$  configuration; (c) the  $1h_{9/2}$  configuration. See the text for further details.

$$\langle I_i, 1/2 | \mathbf{T}(E2) | I_f, 1/2 \rangle = (2I_i + 1)^{1/2} (5/16\pi)^{1/2} \langle I_i, 1/2, 2, 0 | I_f, 1/2 \rangle eQ_0 X, \quad (1.19)$$

where

$$X = 1 + \zeta [(I_i - 1/2)^{1/2} (I_i + 3/2)^{1/2} \langle I_i, 3/2, 2, -1 | I_f, 1/2 \rangle + (I_i + 1/2) \langle I_i, -1/2, 2, +1 | I_f, 1/2 \rangle], \quad (1.20)$$

$\zeta$  is a parameter, and the expressions ' $\langle | \rangle$ ' are CG coefficients: the derivation of equation (1.20) is explained later in the series. An example of high-precision data for  $E2$  properties is available for the nucleus  $^{239}\text{Pu}$  and this is illustrated in figure 1.15. Note that the modification of the  $E2$  matrix elements by the rotation-particle coupling term produces a convergence between the model and the experimental data. Thus, a simple correction to the zeroth-order manifestation of the model leads to an improved description of the data.

We make an important philosophical point in view of the agreement between data and the simple rotational model being used herein: namely, a symmetric top with an  $\mathbf{I} \cdot \mathbf{j}$  particle-rotor coupling. When agreement between a model and data is 'good' in zeroth order and converges to 'very good' when the first-order model correction is

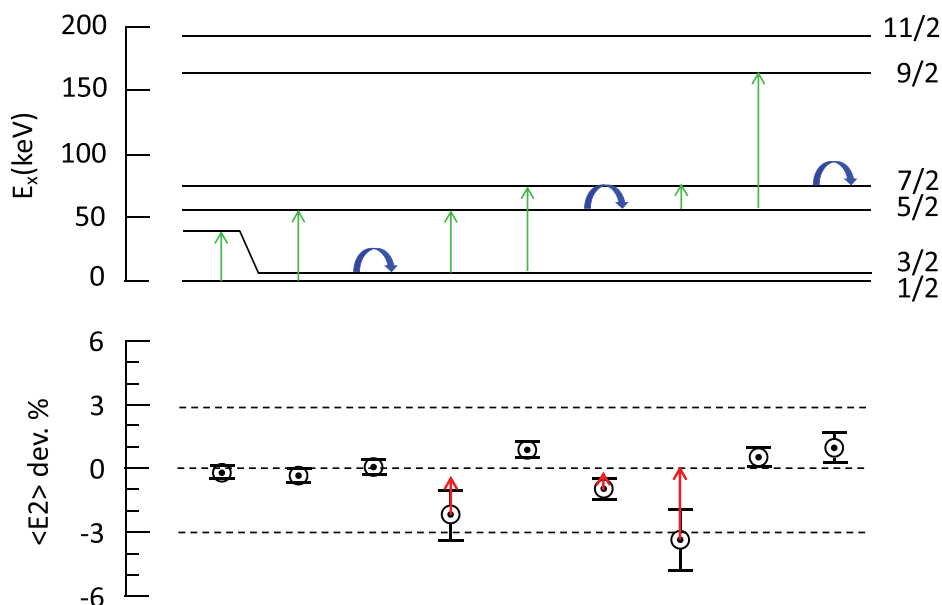


**Figure 1.15.** Deviation from the symmetric rigid rotor of experimental  $E2$  matrix elements (in eb), determined using muonic x-ray spectroscopy, for the  $K = 1/2$  ground-state band in  $^{239}\text{Pu}$ . The red arrows show the changes produced by including RPC effects in the symmetric rotor description (other matrix elements change by less than 0.4%). The data are taken from [17]. The upper part of the figure shows diagonal  $E2$  matrix elements as blue (curved) arrows and off-diagonal  $E2$  matrix elements as green arrows. The zeroth-order fit uses a single parameter,  $Q_0 = 11.592$  b; the fit with RPC effects uses two parameters,  $Q_0 = 11.583$  b and  $\zeta = -1.8 \times 10^{-3}$ , see text, equations (1.13), (1.19) and (1.20). The figure design is a copy of one appearing in the above-cited paper.



made, one must consider this to be a valid fundamental feature of the many-body system. Even if the example is rare, it is unlikely to be an accidental occurrence.

We emphasize, again, the evident validity of the  $K$  quantum number, which in odd nuclei is not zero. Indeed, one can explore the implied values of  $K$  manifested in the  $E2$  matrix elements by ‘reverse engineering’ the reduction process involved in the Wigner–Eckart theorem, i.e. imposing a fixed value of  $Q_0$  for a rotational band and extracting the reduction factors—the CG coefficients. We extend this perspective to transitions between bands later.

Energies for  $K = 1/2$  bands and bands in odd–odd nuclei are handled later. There are almost no  $E2$  data for bands over extended ranges of spin in deformed odd–odd nuclei and excited bands in deformed odd nuclei. Thus, for multiple rotational bands, in a single nucleus, there is a lack of data for exploring whether  $Q_0$  is a universal feature for multiple bands, or if each band is characterized by a different  $Q_0$  value. This lack of data is due to the difficulty of obtaining a ‘clean’ view of the population and subsequent de-excitation of a given excited state in a nucleus. Unless the population of the given state is simple, it becomes (nearly) impossible to deconvolute the feeding ‘history’ of the state. The feeding history must be determined to allow for delays in feeding: this is handled using the so-called Bateman equations.

## 1.4 A wider look at rotation in nuclei: energies and moments of inertia

One can look at energy patterns beyond equation (1.1) via scaling of rotational band energies in even nuclei by  $E(2_1^+)$ . This received a limited inspection in figure 1.4. But in the finer details, a remarkable feature emerges, as presented in table 1.2 for the comparison of  $^{174}\text{Yb}$  and  $^{242}\text{Pu}$ : when scaled, the transition energies between states in the ground-state rotational bands are all identical to within a few parts in a thousand, independent of spin. Further, when considering experimental uncertainties, there is the possibility that these scaled energies are even more similar. We emphasize, these are supposedly complex many-body quantum systems with 174 and 242 bodies, respectively, with very different ‘orbital occupancies’ for the constituent nucleons. Indeed, similar patterns emerge when numerous ground-state bands are scaled in this manner. We note that these scaled energies are closer than any available phenomenological descriptions. There is no known explanation of this, i.e. at the level of the behaviour of nucleons in the nucleus.

The simplest interpretation of energy patterns for bands in nuclei is that the nuclei are deformed, and the energies of band members are characterized by a moment of inertia parameter. From knowledge of the mass, size and deformation of a given nucleus, a classical moment of inertia can be calculated. For a nucleus with

$$R(\theta, \phi) = R[1 + g + \beta Y_{20}(\theta, \phi)], \quad (1.21)$$

$g = -\beta^2/4\pi$  (volume conservation), we obtain

$$Q_0 = 3/\sqrt{(5\pi)} ZeR^2\beta(1 + \sqrt{(5\pi)}\beta/8 + 5\beta^2/8\pi - (5/\pi)^{3/2}\beta^3/192 + \dots), \quad (1.22)$$

**Table 1.2.** Comparison of ground-state band transition energies for  $^{242}\text{Pu}$  and  $^{174}\text{Yb}$ . The data are taken from ENSDF.

$I_i$	$E(^{242}\text{Pu})$ (keV)	$E(^{174}\text{Yb})$ (keV) $\times 0.5824$	$E(^{174}\text{Yb})$ (keV)	% dev.
2	44.54 <sup>2</sup>	44.54 [norm.]	76.471 <sup>1</sup>	–
4	102.8 <sup>1</sup>	102.9	176.645 <sup>2</sup>	+0.098
6	159.0 <sup>1</sup>	158.9	272.918 <sup>6</sup>	–0.063
8	211.7 <sup>4</sup>	211.8	363.64 <sup>5</sup>	+0.047
10	260.5 <sup>6</sup>	260.4 <sup>6</sup>	447.2 <sup>10</sup>	–0.038
12	305.8 <sup>8</sup>	305.4 <sup>8</sup>	524.4 <sup>13</sup>	–0.131
14	347.3 <sup>10</sup>	347.1 <sup>10</sup>	595.9 <sup>17</sup>	–0.058
16	385.0 <sup>11</sup>	384.4 <sup>11</sup>	660 <sup>2</sup>	–0.156
18	419.3 <sup>12</sup>	418.7 <sup>17</sup>	719 <sup>3</sup>	–0.143
20	450.2 <sup>13</sup>	450.8 <sup>29</sup>	774 <sup>5</sup>	+0.133
				–0.035 (avg.)

whence

$$91.7436 Q_0 / Z A^{2/3} = \beta + 0.157\,70\beta^2 + 0.198\,94\beta^3 - 0.010\,457\beta^4. \quad (1.23)$$

Then, using

$$\mathcal{I}_{\text{rigid}} = 2/5AMR^2 \left\{ 1 + \sqrt{(5/16\pi)}\beta + 0.44\beta^2 \right\}, \quad (1.24)$$

where  $M$  is the mass of the nucleon and  $R = 1.2A^{1/3}$  fm,

$$\mathcal{I}_{\text{rigid}} = 9.6405 \times 10^{-58} A^{5/3} \left\{ 1 + 0.3154\beta + 0.44\beta^2 \right\} \quad (1.25)$$

in  $\text{kg m}^2$ . From equation (1.1), with  $A = \hbar^2/2\mathcal{I}_{\text{expt}}$ , where recall that  $1 \text{ J} = 6.241\,509 \times 10^{18} \text{ eV}$ ,

$$\mathcal{I}_{\text{expt}} = 2.0824 \times 10^{-52} / E(2_1^+ \text{ keV}) \quad (1.26)$$

in  $\text{kg m}^2$ . Values for  $\mathcal{I}_{\text{rigid}}$  and  $\mathcal{I}_{\text{expt}}$  are compared below in table 1.3.

There are rotational bands with near constant energy differences for transition energies. Some superdeformed bands exhibit this: one of the best examples is shown in figure 1.16. This depicts a superdeformed band in  $^{152}\text{Dy}$  via observed gamma-ray transition energies. The notable feature is the extraordinary constancy of the differences between these gamma-ray energies: an enhanced view is depicted at the bottom of the figure.

The consequences of equations (1.21)–(1.26) for ground-state bands in  $^{174}\text{Yb}$  and  $^{242}\text{Pu}$ , and for the superdeformed band in  $^{152}\text{Dy}$ , are given in table 1.3.

The results manifested in table 1.3 are profound with respect to the physics of nuclear rotation. It means that nuclei probably approach rigid rotation asymptotically as deformation increases; and the rigid rotation limit is manifestly reached in

**Table 1.3.** Moments of inertia for ground-state rotational bands of a rare earth and an actinide nucleus and for a superdeformed rotational band. The moments of inertia are given in units of  $\text{kg m}^2 \times 10^{-54}$  and the  $2^+$  energies are given in keV. Note that the  $2^+$  energy given for  $^{152}\text{Dy}$  is an estimate based on extrapolation of values observed in association with spins  $>24$ , cf figure 1.16 and equation (1.31). See the text for other details and remarks.

Z	$Q_0$	$A^{2/3}$	$\beta$	$\mathcal{J}_{\text{rigid}}$	$E(2_1^+)$	$\mathcal{J}_{\text{expt}}$	$\frac{\mathcal{J}_{\text{expt}}}{\mathcal{J}_{\text{rigid}}}$	
	(b)			( $\text{kg m}^2$ )	(keV)	( $\text{kg m}^2$ )		
$^{174}\text{Yb}$	70	$7.82^5$	31.167	0.3081	$5.955 \times 10^{-54}$	$76.471^1$	$2.723 \times 10^{-54}$	0.4573
$^{242}\text{Pu}$	94	$11.90^6$	38.834	0.2823	$10.184 \times 10^{-54}$	$44.54^2$	$4.675 \times 10^{-54}$	0.4591
$^{152}\text{Dy}$	66	$17.5^2$	28.482	0.7076	$6.025 \times 10^{-54}$	33.75	$6.170 \times 10^{-54}$	1.024

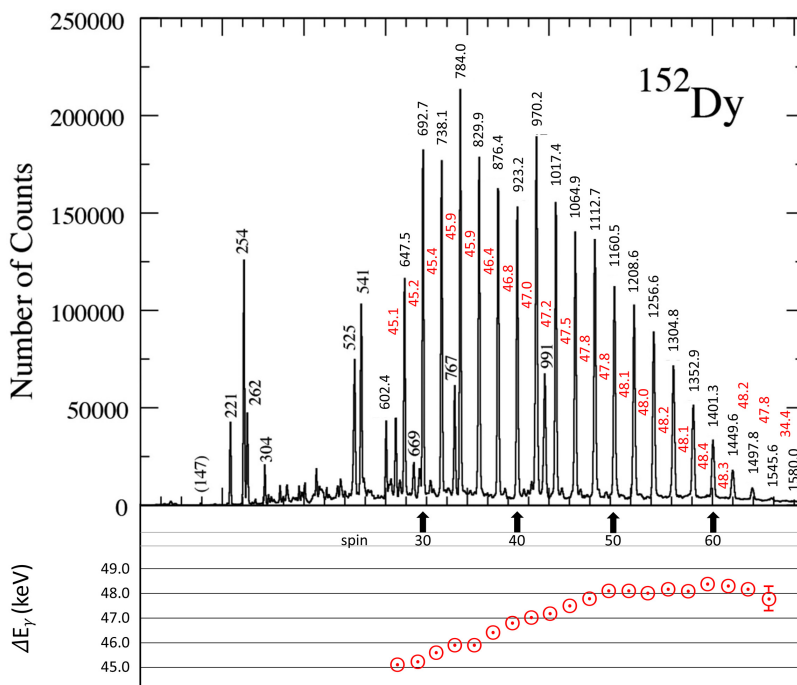


**Figure 1.16.** Example of a superdeformed band manifested in  $^{152}\text{Dy}$ . The figure shows the gamma-ray spectrum associated with the band and the transition energies in keV. Probable spin assignments to the levels from which the gamma rays originate are indicated. The remarkable constancy of the differences between successive gamma rays is depicted at the bottom of the figure. Uncertainties in the gamma-ray energies are generally less than the size of the data points, except the right-hand-most point. Further details are discussed in the text. Note, the de-exciting cascade of gamma rays is attenuated starting around spin 30 due to decay out of the band into lower-lying high-spin states, sometimes called ‘draining’; this is beyond the scope of the present discussion. The spectrum was provided courtesy of T Lauritsen and is based on a similar spectrum appearing in [18]. Other data are taken from ENSDF. Reproduced from [23]. Copyright 2010 World Scientific Publishing Company.

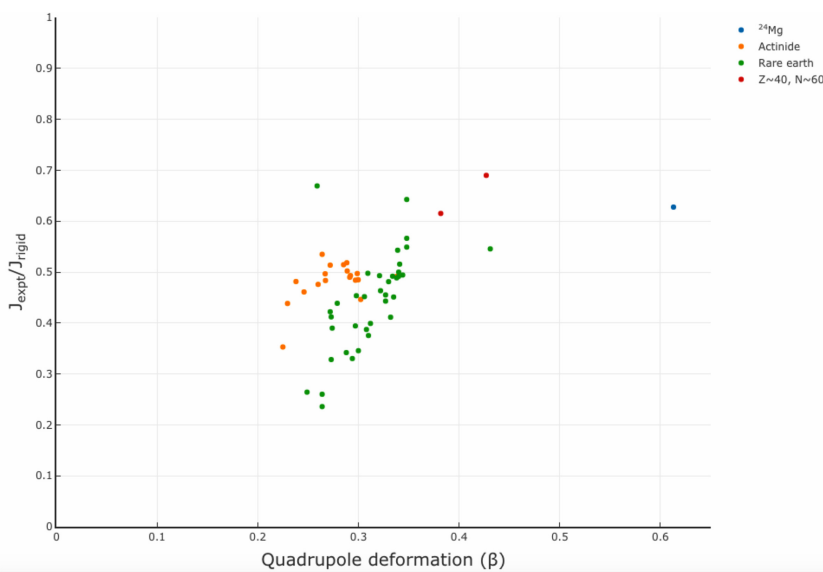


**Figure 1.17.** Selected view of nuclear moments of inertia for nuclei which exhibit a rotational band built on their ground state. Moments of inertia are presented as a ratio of the experimental moment of inertia deduced from the excitation energy of the  $2^+$  state (equation (1.1)) with  $A = \hbar^2/2\mathcal{J}_{\text{expt}}$ , divided by the rigid body moment of inertia (equation (1.24)), plotted as a function of the quadrupole deformation,  $\beta$  for the relevant isotopes. Data are presented for the rare earth isotopes, the actinide region, the region close to  $Z \sim 40$ ,  $N \sim 60$  and for  $^{24}\text{Mg}$ . Interactive version available in e-book which can be downloaded from <http://iopscience.iop.org/book/mono/978-0-7503-5643-5>.

some nuclei. We caution that this derivation is based on a naïve view of the nucleus as a quadrupole-deformed constant-density extended object with a sharp surface, i.e. no allowance is made for surface diffuseness or higher multipole deformations of the nucleus. We look at higher multipole deformations later. Figure 1.17 presents moments of inertia, extracted using these simple prescriptions, for selected nuclei. We do not comment on the remarkable similarity of  $\mathcal{J}_{\text{expt}}/\mathcal{J}_{\text{rigid}}$  for  $^{174}\text{Yb}$  and  $^{242}\text{Pu}$ , except to note that this would appear to be independent of the near-identical scaled-energy patterns shown in table 1.2.

There is considerable confusion over moments of inertia extracted from rotational bands in odd-mass nuclei: the origin is in the use of equation (1.1), modified for excitation and spin of a given band head, viz.

$$E = E_0 + AI(I + 1), \quad (1.27)$$

where  $I = K, K + 1, K + 2, \dots$  and the excitation of the band head is given by  $E_0 + AK(K + 1)$ . It is essential to include the rotation-particle coupling term when making deductions about moments of inertia in odd nuclei. From plots such as depicted in figures 1.11(a)–(d) *et seq.* a useful relationship for replacement of equation (1.27) would take the form

$$E = E_0 + A(I - \alpha)(I - \alpha + 1), \quad (1.28)$$

where  $\alpha$  is the horizontal displacement in spin between the odd-mass nucleus and the neighbouring even–even ‘core’ nucleus. Thus, e.g. in figure 1.13 a,  $\alpha = 2.8$  at  $I_i = 13/2$ . Such a relationship, to our knowledge, has never received attention in the literature; although it has been suggested [19], this was without exploration at the level of presentation of data such as shown herein. It is immediately evident that extracting an ‘ $A$ ’ parameter from data will give different values depending on whether equation (1.27) or (1.28) is used. Note that if single energy differences are used one arrives at the relationship

$$\Delta E_{I,I-2} = E_\gamma = A(4I - 2) \quad (1.29)$$

from equation (1.27) and

$$\Delta E_{I,I-2} = E_\gamma = A(4I - 4\alpha - 2) \quad (1.30)$$

from equation (1.28); whereas if double energy differences are used (employing states with spins  $I$ ,  $I - 2$ , and  $I - 4$ ) one arrives at the relationship

$$\Delta^2 E = \Delta E_\gamma = 8A. \quad (1.31)$$

This is universally manifested in odd-mass bands and the ground-state bands of neighboring even–even ‘core’ nuclei, as illustrated in figures 1.11(a)–(d) *et seq.* Commonly, use of equations (1.29) and (1.31) has led to the terminology ‘type-I’ and ‘type-II’ moments of inertia, respectively. We leave this issue without further comment.

There is a further puzzling feature manifested in the comparison of rotational bands in odd-mass nuclei with ground-state bands in even-mass nuclei: the unpaired nucleon should exhibit a ‘Coriolis effect’ whereby the ‘alignment’ of its spin,  $j$  with the core angular momentum,  $R$  should progressively increase with increasing total spin, i.e. the semi-classical angle in equation (1.18) should ‘close’. This is not observed. The patterns manifested in figures 1.11–1.13, to lowest order, show a constant alignment, i.e., there is no classic rotational alignment effect such as occurs with gyroscopes. Thus, one must question even the idea that the nucleus is ‘rotating’ in the classical sense when rotation-alignment effects (Coriolis effects) are not conforming to classical patterns.

We note that the above empirical patterns have not been addressed theoretically at a foundational level. Discussion can be found in the literature regarding some of the effects portrayed; but attempts to explain such data have been confined to the naïve rotor model. The result has been to invoke ‘delicate cancellations’ involving ‘blocking of pairing-correlation effects’, ‘deformation-driving effects’, and ‘rotation-alignment effects’ due to the unpaired nucleon. We express the view that fine-tuning model parameters on a case-by-case basis to fix discrepancies with data is the signature of the much-discussed<sup>7</sup> ‘need for a paradigm shift’ in science.

---

<sup>7</sup>The expression ‘a paradigm shift’ was first coined by Thomas S Kuhn in [24]. We add, as authors we did not foresee this paradigm shift, we have only assembled data and noted systematic patterns. We do not offer any theoretical insights beyond recommending that the naïve rotor model, while useful for organizing data and describing  $E2$  properties of nuclei, should not be the basis for refining exploration of rotational energies in nuclei. We discuss this in more detail later.

A summary view of the data presented can be made with a few key points. Where data are available, in nuclei that can be described as well-deformed, the simplest rotor model is realized at the level of 1%–2% in electromagnetic properties; in nuclei that can be described as superdeformed, the simplest rotor model is realized at the few percent level with respect to rigid-body rotation with a moment of inertia that matches expectations of classical mechanics. However, the requisite high-precision data are severely lacking. Adopting the view that in complex systems, the emergence of such simple behaviour is not by chance, rather it is a manifestation of asymptotic behaviour, this indicates that much work needs to be done.

## 1.5 Exercises

- 1-1. With reference to table 1.1, for the nuclei shown, tabulate values of  $B_{I,I-2}/B_{20} f(I)$  for  $12 \rightarrow 10$ ,  $14 \rightarrow 12$ , ... transitions using  $B(E2)$  data in ENSDF. Note: use equation (1.6) to determine  $f(12)$ ,  $f(14)$ , ...
- 1-2. Make a similar table to table 1.1 for the actinide isotopes shown in figure 1.2 using ENSDF data for  $B(E2)$  values.
- 1-3. Following on from exercise 1-2, find and add other deformed actinide region  $B_{I,I-2}$  data using ENSDF data for  $B(E2)$  values. (Note: the data are very limited and confined to low spin states.)
- 1-4. With reference to table 1.2, using data in ENSDF, explore deformed rare earth and actinide region nuclei for similar scaled rotational transition energies in even–even nuclei. As a set of useful starting nuclei, we suggest:  $^{156}\text{Nd}$ ,  $^{158,160}\text{Sm}$ ,  $^{240,242}\text{Pu}$ ,  $^{172,174}\text{Yb}$ ,  $^{168,170}\text{Er}$ ,  $^{180}\text{Hf}$ ; then look at  $^{160}\text{Gd}$ ,  $^{162,164}\text{Dy}$ ,  $^{166}\text{Er}$ ,  $^{170,176}\text{Yb}$ ,  $^{182}\text{W}$ ,  $^{234,236,238}\text{U}$ ,  $^{236,238}\text{Pu}$ .
- 1-5. Test the rotational energy formula, equation (1.3), for the nuclei presented in table 1.2.
- 1-6. Using equation (1.12), obtain the  $Q_0^{\text{gs}}$  values in figures 1.7(a)–(f) from the  $Q_s^{\text{gs}}$  values given in ENSDF.
- 1-7. With reference to figure 1.11, for  $E_\gamma$  versus  $I_i$  using data in ENSDF, make similar plots for rotational bands built on the Nilsson configuration  $7/2^+$  [404]. As a set of useful starting nuclei, we suggest odd-mass Lu and Ta isotopes where this Nilsson configuration forms the ground-state bands.
- 1-8. For the nucleus  $^{157}\text{Tb}$ , make a plot of  $E_\gamma$  versus  $I_i$ , of those shown in figures 1.11–1.13, for the Nilsson configuration  $5/2^-$  [532]. Comment on the statement in the narrative that alignment effects increase with the decreasing value of the Nilsson quantum number  $\Omega$ , by comparing with figure 1.12 and noting that  $5/2^-$  [532],  $7/2^-$  [523] and  $9/2^-$  [514] all have the spherical parentage configuration  $h_{11/2}$ , i.e.  $j = 11/2$ . (Use the data given in ENSDF for  $^{157}\text{Tb}$ , where note that the head of the  $5/2^-$  [532] band is at 326.3 keV.)
- 1-9. For the scaling  $Q_0/ZR^2$ , compare typical rare earth nuclei (figures 1.8 and 1.9) and actinide nuclei (figure 1.10)  $Q_0$  values. Use  $R = 1.2A^{1/3}$  fm. Estimate the  $Q_0$  values by inspection of the figures.

- 1-10. If  $j$  is parallel to  $I$ , for an even–even neighbouring ‘core’ band with  $I = 0, 2, 4, 6, \dots$ , sketch what a plot of  $E_\gamma$  versus  $I_i$  will look like in an odd-mass nucleus compared to the neighbouring even–even nucleus.
- 1-11. Derive equation (1.9) from equations (1.4), (1.5), and (1.8). Note, a Clebsch–Gordan coefficient calculator is available on Wolfram Alpha (<https://www.wolframalpha.com/input?i=Clebsch-Gordan+calculator>).
- 1-12. Look for superdeformed bands that exhibit near constant differences in transition energies such as illustrated in figure 1.16 for  $^{152}\text{Dy}$ . Relevant data can be obtained from [20].
- 1-13. Explore fitting equation (1.28) to odd-A nuclei. Start with the nuclei in figure 1.13 and use values of  $\alpha$  given by the numbers in the black boxes, e.g.  $\alpha = 2.2$  for  $^{173}\text{Yb}$ . How do the fits compare with using equation (1.27)?
- 1-14. There is a simple empirical correlation between  $B(E2: 0_1^+ \rightarrow 2_1^+)$  values and the excitation energy of the first excited  $2^+$  state,  $E(2_1^+)$ , called the Grodzins relationship [21], viz.

$$B(E2: 0_1^+ \rightarrow 2_1^+) \times E(2_1^+) \times \frac{A}{Z^2} \sim \text{constant}. \quad (1.32)$$

This is often employed with the dimensions of  $B(E2)$  in  $\text{e}^2\text{b}^2$  and  $E(2)$  in keV, whence the constant for many nuclei is about 16. Note that **ENSDF** usually gives  $B(E2)$  as  $B(E2; 2_1^+ \rightarrow 0_1^+)$  in W.u.; recall  $B(E2: 0_1^+ \rightarrow 2_1^+) = 5 \times B(E2; 2_1^+ \rightarrow 0_1^+)$ , cf equation (1.4) (the spin factor in the denominator). The relationship between  $B(E2)$  values in W.u. and  $\text{e}^2\text{b}^2$  is given by  $1 \text{ W.u.} = 5.940 \times 10^{-6} A^{4/3} \text{ e}^2\text{b}^2$ . The  $B(E2; 0_1^+ \rightarrow 2_1^+)$  values in  $\text{e}^2\text{b}^2$  are compiled in [22].  $E(2)$  values in keV are given in **ENSDF**.

For example, for  $^{174}\text{Yb}$ :  $5.85 \times 76.471 \times 174/70^2 = 15.9$ . The **ENSDF** value for  $^{174}\text{Yb}$   $B(E2; 2_1^+ \rightarrow 0_1^+)$  is 201 W.u.:  $201 \times 5 \times 5.94 \times 10^{-6} \times 174^{4/3} = 5.71 \text{ e}^2\text{b}^2$ . This value is superseded by the value of  $5.85 \text{ e}^2\text{b}^2$  given in [22].

Explore the Grodzins relationship using data from **ENSDF**: for example, look at local mass regions to determine the constancy of the product; compare this product for nuclei at closed shells with nuclei in mid-open shell regions.

- 1-15. Preamble: the following notes and exercises are at a level considerably more advanced than the preceding exercises. For the less specialized reader it is sufficient to treat Clebsch–Gordan coefficients as numbers that can be obtained using the Wolfram Alpha website. We illustrate in the following how to derive algebraic expressions for  $E2$  properties presented in this chapter starting from more general equations given in [10]. We recognize that a typical experimentalist will likely start with data and the equations provided, and reach a familiarity of the effectiveness of the equations without initial concern for their origin<sup>8</sup>. Curiosity may then

<sup>8</sup>We note that the famous equation,  $E = mc^2$  is widely used, but its derivation is a mystery to many.

lead the reader to the origin of the equations below, which in turn have been derived by methods which are presented from first principles, i.e. derivation of the equations given in appendix A, in [10].

The Clebsch–Gordan coefficients that appear in equations (1.5) and (1.7) can be obtained from appendix A, table A.4 of [10] which gives expressions for  $\langle j_1 m_1 2 m_2 | j m \rangle$ . We delay some substitution of assigned values so that the origins of the terms can be seen in [10].

For  $j = j_1 - 2$ ,  $m_2 = 0$ ,  $m_1 = m$ , and

$$\langle j_1 m 2 0 | j m \rangle = \frac{\sqrt{3(j-m+2)(j-m+1)(j+m+2)(j+m+1)}}{\sqrt{(2j_1-2)(2j_1-1)j_1(2j_1+1)}}, \quad (1.33)$$

then, for  $j_1 = I$ ,  $m = 0$ ,  $j = I - 2$  and

$$\begin{aligned} \langle I 0 2 0 | I - 2, 0 \rangle &= \frac{\sqrt{3I(I-1)I(I-1)}}{\sqrt{2(I-1)(2I-1)I(2I+1)}} \\ &= \frac{\sqrt{3I(I-1)}}{\sqrt{2(2I-1)(2I+1)}}. \end{aligned} \quad (1.34)$$

For  $j = j_1$ ,  $m_2 = 0$ ,  $m_1 = m$ , and

$$\langle j_1 m 2 0 | j m \rangle = \frac{3m^2 - j(j+1)}{\sqrt{(2j_1-1)j_1(j_1+1)(2j_1+3)}}, \quad (1.35)$$

then, for  $j = j_1 = I$ ,  $m = 0$ ,

$$\begin{aligned} \langle I 0 2 0 | I 0 \rangle &= \frac{-I(I+1)}{\sqrt{(2I-1)I(I+1)(2I+3)}} \\ &= -\frac{\sqrt{I(I+1)}}{\sqrt{(2I-1)(2I+3)}}, \end{aligned} \quad (1.36)$$

and for  $j_1 = I$ ,  $m = I$ ,  $j = I$

$$\begin{aligned} \langle I I 2 0 | I I \rangle &= \frac{3I^2 - I(I+1)}{\sqrt{(2I-1)I(I+1)(2I+3)}} \\ &= \frac{I(2I-1)}{\sqrt{(2I-1)I(I+1)(2I+3)}} \\ &= \frac{\sqrt{I(2I-1)}}{\sqrt{(I+1)(2I+3)}}. \end{aligned} \quad (1.37)$$

- (a) From equation (1.34), obtain  $\langle 2020|00 \rangle = \frac{1}{\sqrt{5}}$ .
- (b) From equation (1.34), obtain equation (1.6).



- (c) From equations (1.7), (1.36) and (1.37), obtain equation (1.8).
- (d) From equation (1.35) with  $j = j_1 = I$ ,  $m = K$  and equation (1.37), adapting equation (1.7) by the replacement  $\langle I, K=0 | T(E2) | I, K=0 \rangle \rightarrow \langle I, K | T(E2) | K \rangle$ , obtain equation (1.12).
- (e) The factor  $(5/16\pi)^{1/2}$  that appears in equation (1.5) (and following equations) is because the electric quadrupole moment of a nucleus is defined as

$$\langle Q \rangle = (16\pi/5)^{1/2} \sum_{\text{nucleons}, i} e_{\text{eff}}^i r_i^2 Y_{20}(\theta_i, \psi_i), \quad (1.38)$$

where  $(\theta_i, \psi_i)$  are polar coordinates defined with respect to the centre of mass of the nucleus,  $Y_{20}$  is a spherical harmonic, and  $e_{\text{eff}}$  allows for effective charges on the proton and neutron. Show that the factor  $(16\pi/5)^{1/2}$  ensures that the total charge in a nucleus is equal to  $+Ze$ , where  $Z$  is the number of protons (here assume  $e_{\text{eff}}^{\text{proton}} = +1e$  and  $e_{\text{eff}}^{\text{neutron}} = 0$ ).

## A View of Nuclear Data

### 1. Some preliminary views of nuclei

In anticipation of addressing simple features observed in nuclear data, some simple criteria of physics philosophy are introduced.

Notably, some basic quantum mechanical concepts are sketched.

The use of models for handling complex many-body systems is noted.

Caution is advised with respect to imposing ideas from familiar avenues of physics



**Tutorial 1.1** Some preliminary views of nuclei. The video can be downloaded from <https://doi.org/10.1088/978-0-7503-5643-5>.

---

## A View of Nuclear Data

### Nuclear rotation: a first look

#### 2. Electric quadrupole, E2 properties

The most remarkable emergent phenomenon encountered in nuclear structure study is deformation and rotation

The primary experimental view of nuclei is  $\gamma$ -ray spectroscopy: the  $\gamma$ -ray portion of the electromagnetic spectrum is dictated by elementary quantum mechanical energy estimates.

Nuclei can be regarded as distributions of electrical charge that act as "antennae" coupled to em fields.

The most extraordinary emergent feature of nuclear rotation is the simplicity of the em coupling strengths. There are now sufficient data to argue that nuclear charge distributions appear to be (near) rigid as a function of increasing angular momentum, i.e. nuclei do not behave like liquid drops.

However, simple rotational model estimates of energies do not agree with observation. This is not understood.

The simplest rotor model provides the necessary quantum mechanics to understand basic nuclear



---

**Tutorial 1.2** E2 properties. The video can be downloaded from <https://doi.org/10.1088/978-0-7503-5643-5>.

## A View of Nuclear Data

### Nuclear rotation: a first look

#### 3. Excitation energies in even-even nuclei

Electromagnetic matrix elements of deformed nuclei support (near) rigid intrinsic quadrupole moments, but energies do not support a fixed moment of inertia : this is a fundamental contradiction

However rotational energy patterns of deformed nuclei, even though not matching the  $I(I+1)$  spin dependence of a symmetric top, exhibit smooth variations with spin.

Some nuclei also exhibit energy patterns, which when scaled, are identical to within  $\sim 0.1\%$  over wide spin ranges.

Generally, moments of inertia have values that are about  $\sim 50\%$  of classical rigid-body values.

So-called superdeformed bands possibly have moments of inertia equal to the classical value.



**Tutorial 1.3** Excitation energies in even-even nuclei. The video can be downloaded from <https://doi.org/10.1088/978-0-7503-5643-5>.

## A View of Nuclear Data

### Nuclear rotation: a first look

#### 4. Excitation energies in odd-mass nuclei

Rotations of odd-mass nuclei necessitate a simple model: the rotation-particle coupling model.  
This is expressed as

$$I = R + J,$$

where  $I$  is the total nuclear spin,  $R$  is the rotational angular momentum and  $J$  is the total spin of the particle.

The model leads to an  $I \cdot J$  energy term which is sometimes called the “Coriolis” term because it resembles the classical analog.

Contributions of this term to rotational energies in odd-mass nuclei are either zero or a constant value.

Consequently, there appear to be no Coriolis effects in nuclei



**Tutorial 1.4** Excitation energies in odd mass nuclei. The video can be downloaded from <https://doi.org/10.1088/978-0-7503-5643-5>.

## A View of Nuclear Data

### Nuclear rotation

#### 5. Further look at excitation energies in odd-mass nuclei

Concepts of “alignment-energy” and “alignment-spin” emerge from data.

This leads to concepts of “deformation-alignment” (Nilsson model) and “rotation-alignment” as competing energy factors.



**Tutorial 1.5** Further look at excitation energies in odd-mass nuclei. The video can be downloaded from <https://doi.org/10.1088/978-0-7503-5643-5>.

## A View of Nuclear Data

### Comprehensive (complete) spectroscopy 18. Multi-spectroscopy study: $^{152}\text{Sm}$



$^{152}\text{Sm}$  has been the subject of a coordinated program of study using a variety of spectroscopic techniques.

The various spectroscopic types are pictorially illustrated.

Details are limited to visual illustration, i.e. technical details of analysis are omitted.

Key insights into the structure of  $^{152}\text{Sm}$  are noted.

[This is a program being pursued by JLW in collaboration with Paul Garrett (Univ. of Guelph); and in its early stages, with W. David Kulp (when he was at Georgia Tech.).]

P.E. Garrett et al., J. Phys. G: Nucl. Part. Phys. **31** S1855 (2005)  
W.D. Kulp et al., Phys. Rev. C **76** 034319 (2007)  
W.D. Kulp et al., Phys. Rev. C **77** 061301(R) (2008)  
P.E. Garrett et al., Phys. Rev. Lett. **103** 062502 (2009)

**Tutorial 1.6** Comprehensive spectroscopy: Multi-spectroscopy study:  $^{152}\text{Sm}$ . The video can be downloaded from <https://doi.org/10.1088/978-0-7503-5643-5>.

## A View of Nuclear Data

### Comprehensive (complete) spectroscopy 18. Multi-spectroscopy study: $^{152}\text{Sm}$



$^{152}\text{Sm}$  has been the subject of a coordinated program of study using a variety of spectroscopic techniques.

The various spectroscopic types are pictorially illustrated.

Details are limited to visual illustration, i.e. technical details of analysis are omitted.

Key insights into the structure of  $^{152}\text{Sm}$  are noted.

[This is a program being pursued by JLW in collaboration with Paul Garrett (Univ. of Guelph); and in its early stages, with W. David Kulp (when he was at Georgia Tech.).]

P.E. Garrett et al., J. Phys. G: Nucl. Part. Phys. **31** S1855 (2005)  
W.D. Kulp et al., Phys. Rev. C **76** 034319 (2007)  
W.D. Kulp et al., Phys. Rev. C **77** 061301(R) (2008)  
P.E. Garrett et al., Phys. Rev. Lett. **103** 062502 (2009)

**Tutorial 1.6** (Continued.). The video can be downloaded from <https://doi.org/10.1088/978-0-7503-5643-5>.

# A View of Nuclear Data

## Comprehensive (complete) spectroscopy

### 18. Multi-spectroscopy study: $^{152}\text{Sm}$


$^{152}\text{Sm}$  has been the subject of a coordinated program of study using a variety of spectroscopic techniques.

The various spectroscopic types are pictorially illustrated.

Details are limited to visual illustration, i.e. technical details of analysis are omitted.

Key insights into the structure of  $^{152}\text{Sm}$  are noted.

[This is a program being pursued by JLW in collaboration with Paul Gar  
and in its early stages, with W. David Kulp (when he was at Geor



P.E. Garrett et al., J. Phy  
W.D. Kulp et al., Phys. R  
W.D. Kulp et al., Phys. Rev. C **11** 061304 (1974) (2008)  
P.E. Garrett et al., Phys. Rev. Lett. **103** 062502 (2009)

**Tutorial 1.6** (Continued.). The video can be downloaded from <https://doi.org/10.1088/978-0-7503-5643-5>.

# A View of Nuclear Data

## Comprehensive (complete) spectroscopy

### 18. Multi-spectroscopy study: $^{152}\text{Sm}$

$^{152}\text{Sm}$  has been the subject of a coordinated program of study using a variety of spectroscopic techniques.

The various spectroscopic types are pictorially illustrated.

Details are limited to visual illustration, i.e. technical details of analysis are omitted.

Key insights into the structure of  $^{152}\text{Sm}$  are noted.

[This is a program being pursued by JLW in collaboration with Paul G  
and in its early stages, with W. David Kulp (when he was at Ge



P.E. Garrett et al., J. P  
W.D. Kulp et al., Phys  
W.D. Kulp et al., Phys  
P.E. Garrett et al., Phys. Rev. Lett. **103** 062502 (2009)

**Tutorial 1.6** (Continued.). The video can be downloaded from <https://doi.org/10.1088/978-0-7503-5643-5>.

## References

- [1] Karamatskos E T *et al* 2019 Molecular movie of ultrafast coherent rotational dynamics of OCS *Nat. Commun.* **10** 3364
- [2] He Y *et al* 2019 Direct imaging of molecular rotation with high-order-harmonic generation *Phys. Rev. A* **99** 053419
- [3] Mizuse K, Fujimoto R, Mizutani N and Ohshima Y 2017 Direct imaging of laser-driven ultrafast molecular rotation *J. Vis. Exp.* **120** e54917
- [4] Hilborn R C and Yuca C L 1996 Spectroscopic test of the symmetrization postulate for spin-0 nuclei *Phys. Rev. Lett.* **76** 2844
- [5] de Angelis M, Gagliardi G, Gianfrani L and Tino G M 1996 Test of the symmetrization postulate for spin-0 particles *Phys. Rev. Lett.* **76** 2840
- [6] Modugno G, Ignuscio M and Tino G M 1998 Search for small violations of the symmetrization postulate for spin-0 particles *Phys. Rev. Lett.* **81** 4790
- [7] DeMille D, Doyle J M and Sushkov A O 2017 Probing the frontiers of particle physics with tabletop-scale experiments *Science* **357** 990–4
- [8] Pastor P C, Galli I, Giusfredi G, Mazzotti D and De Natale P 2015 Testing the validity of bose-einstein statistics in molecules *Phys. Rev. A* **92** 063820
- [9] Jenkins D G and Wood J L 2021 *Nuclear Data: A Primer* (Bristol: IOP Publishing) <https://iopscience.iop.org/book/mono/978-0-7503-2674-2>
- [10] Heyde K and Wood J L 2020 *Quantum Mechanics for Nuclear Structure: An Intermediate Level View* (Bristol: IOP Publishing) <https://iopscience.iop.org/book/mono/978-0-7503-2171-6>
- [11] Heyde K and Wood J L 2020 *Quantum Mechanics for Nuclear Structure: A Primer* (Bristol: IOP Publishing) <https://iopscience.iop.org/book/mono/978-0-7503-2179-2>
- [12] Kusakari H, Oshima M, Uchikura A, Sugawara M, Tomotani A, Ichikawa S, Iimura H, Morikawa T, Inamura T and Matsuzaki M 2000 Erratum: Electromagnetic transition probabilities in the natural-parity rotational bands of  $^{155, 157} \text{Gd}$  *Phys. Rev. C* **63** 029901(E)
- [13] Stone N J 2021 Table of nuclear electric quadrupole moments Technical report *IAEA INDC (NDS)-0833*
- [14] Powers R J, Boehm F, Hahn A A, Miller J P, Vuilleumier J-L, Wang K-C, Zehnder A, Kunselman A R and Roberson P 1977 An experimental study of  $E0$   $E2$  and  $E4$  charge moments of  $^{161} \text{Dy}$  using muonic atoms *Nucl. Phys. A* **292** 487–505
- [15] Zehnder A, Boehm F, Dey W, Engfer R, Walter H K and Vuilleumier J-L 1975 Charge parameters, isotope shifts, quadrupole moments, and nuclear excitation in muonic  $^{170-174, 176} \text{Yb}$  *Nucl. Phys. A* **254** 315–40
- [16] Tanaka Y, Steffen R M, Shera E B, Reuter W, Hoehn M V and Zumbro J D 1984 Measurement and analysis of muonic x rays of  $^{176, 177, 178, 179, 180} \text{Hf}$  *Phys. Rev. C* **30** 350
- [17] Zumbro J D, Naumann R A, Hoehn M V, Reuter W, Shera E B, Bemis C E and Tanaka Y 1986  $E2$  and  $E4$  deformations in  $^{232} \text{Th}$  and  $^{239, 240, 242} \text{Pu}$  *Phys. Lett. B* **167** 383
- [18] Lauritsen T *et al* 2002 Direct decay from the superdeformed band to the yrast line in  $^{152} \text{Dy}_{86}$  *Phys. Rev. Lett.* **88** 042501
- [19] Peker L K, Pearlstein S, Rasmussen J O and Hamilton J H 1984 Strength of Coriolis alignment in actinide nuclei *Phys. Rev. C* **29** 271
- [20] Singh B, Zywna R and Firestone R B 2002 table of superdeformed nuclear bands and fission isomers: 3rd edn (October 2002) *Nucl. Data Sheets* **97** 241–592
- [21] Grodzins L 1962 The uniform behaviour of electric quadrupole transition probabilities from first  $2^+$  states in even–even nuclei *Phys. Lett.* **2** 88

- [22] Pritychenko B, Birch M, Singh B and Horoi M 2016 tables of  $E2$  transition probabilities from the first  $2^+$  states in even-even nuclei *At. Data Nucl. Data tables* **107** 1–139
- [23] Rowe D J and Wood J L 2010 *Fundamentals of Nuclear Models: Foundational Models* (Singapore: World Scientific)
- [24] Kuhn T S 1962 *The Structure of Scientific Revolutions* (Chicago, IL: University of Chicago Press)